NASA TECHNICAL NOTE

NASA TN D-2619

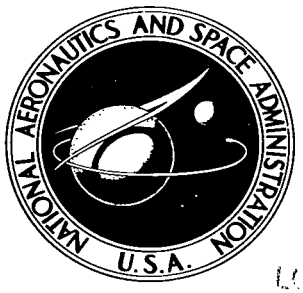

NASA TN D-2619

EXPERIMENTAL INVESTIGATION OF ELECTRIC DRAG ON SPHERICAL SATELLITE MODELS

by William C. Pitts and Earl D. Knechtel

Ames Research Center
Moffett Field, Calif.

NATIONAL AERONAUTICS AND SPACE ADMINISTRATION • WASHINGTON, D. C. • FEBRUARY 1965

EXPERIMENTAL INVESTIGATION OF ELECTRIC DRAG ON SPHERICAL SATELLITE MODELS

By William C. Pitts and Earl D. Knechtel

Ames Research Center
Moffett Field, Calif.

NATIONAL AERONAUTICS AND SPACE ADMINISTRATION

For sale by the Office of Technical Services, Department of Commerce,
Washington, D.C. 20230 -- Price $2.00

EXPERIMENTAL INVESTIGATION OF ELECTRIC DRAG ON SPHERICAL SATELLITE MODELS[1]

By William C. Pitts and Earl D. Knechtel

Ames Research Center
Moffett Field, Calif.

SUMMARY

Electric drag is defined as the difference between the drag of a charged satellite and the drag of an identical satellite with no charge. The drag increment is a consequence of the effective increase in size of the satellite resulting from scattering of ambient ions by the satellite potential. Experimental results of this investigation, wherein electric drag was measured on conducting spheres in a streaming mercury plasma, have shown that electric drag can be a significant portion of the total drag if the fraction ionization is sufficiently high. To properly estimate electric drag of satellites it is necessary to account both for the ion surface collision and for the shielding effect of the ion sheath around the satellite surface. Among the several conflicting theories available, these conditions are most nearly fulfilled by the theory of Jastrow and Pearse. Upon using this theory and the test conditions of this investigation, the drag of 1.9- and 2.5-cm-diameter spheres is predicted to within 10 percent of the experimental results. Scaling parameters developed herein allow the relation of the present experimental results to satellite conditions. The scaling parameters and an existing simple ion sheath theory are used as guides in developing an approximate equation that estimates electric drag to reasonable accuracy over scaling parameter ranges of practical interest.

INTRODUCTION

Earth satellites orbit in a medium composed of ions and electrons, in equal numbers, and neutral atoms. A satellite in such a medium will acquire a net negative charge due to the higher mobility of the electrons. To date, satellite potential measurements have ranged from -0.15 to -4 volts (refs. 1 and 2, respectively). This negative charge gives rise to several forces on the satellite in addition to those caused by gravity, radiation pressure, and impacts with neutral particles. The charge-associated drag forces result from the scattering of atmospheric ions and interaction with the earth's magnetic field. Since satellite drag has bearing on the satellite lifetime and on the determination of atmospheric density from observations of the orbital decay rate, the importance of charge drag relative to other drag forces must be assessed.

[1]A résumé of this paper was published in the AIAA Journal, vol. 2, June 1964, pp. 1148-1151.

Several theories have been published (refs. 3-10) which differ by four orders of magnitude in their prediction of electric drag. Comprehensive reviews of most of these theories are given in references 4 and 11. The large differences in predicted drag are a result of unresolved questions as to the proper choice of theoretical model. The primary differences between models involve the plasma sheath that forms near the satellite surface and the details of the ion-surface interaction. In view of the large differences of opinion regarding the proper formulation of the theoretical model and the resulting orders-of-magnitude differences in estimated effect, it was decided to conduct a laboratory-scale experimental investigation of the effect of satellite charge on drag. The effect of the earth's magnetic field on the drag of a charged satellite was not considered in this investigation because, for most cases in space, induction drag is expected to be small compared to electric drag (ref. 6). In the laboratory tests the electric field was scaled out of proportion to the magnetic field so that the magnetic effects are considered to be small enough not to invalidate the present results.

Laboratory simulation of satellite conditions required a plasma beam having ion mean-free paths much larger than the model dimensions, and a directed ion velocity much larger than the ion thermal velocity but much less than the electron thermal velocity. These conditions were met by an apparatus which provided a broad beam of singly ionized mercury plasma operable over a range of ion energies from 60 to 250 ev. The experiment consisted of measuring the drag force acting on spherical conducting models as the model potential was varied. Measurements were carried out for two model diameters and several ion energies.

SYMBOLS

a	model or satellite radius
B	magnetic field strength
D	total ion drag due to ions, $D_O + D_E$
D_E	electric drag
D_I	impact drag
D_N	neutral particle drag
D_R	reflection drag
D_O	ion drag of uncharged model or satellite
E	ion kinetic energy at infinity (relative to satellite)
e	electron charge

k Boltzmann's constant

n_e electron number density

n_i ion number density

n_∞ ambient number density of ions or electrons

p perpendicular distance between flow axis of symmetry and free-stream velocity vector

p_g value of p for ion trajectory that grazes surface

R dimensionless radius, $\frac{r}{\lambda_D}$

R_o value of R at body surface, $\frac{a}{\lambda_D}$

r radial distance from body center

T_e electron temperature

v_i ion velocity

v_s satellite velocity

δ thickness of simplified ion sheath

θ inclination of ion radius vector from the axis of symmetry

λ_D Debye radius, $\sqrt{kT_e/4\pi ne^2}$

ρ charge density

Φ dimensionless parameter, $\frac{r}{\lambda_D}\frac{e\varphi}{kT_e}$

Φ_o value of Φ at body surface, $\frac{a}{\lambda_D}\frac{e\varphi_o}{kT_e}$

φ electrical potential referred to free space

φ_o value of φ at body surface

THEORETICAL CONSIDERATIONS

Physical Description of Electric Drag

The satellite environment is shown conceptually in figure 1. For altitudes of interest the satellite orbits in a medium composed of ions, electrons, and neutral atoms. The prevailing types of ions and atoms depend on the altitude (refs. 12 and 13). At low altitudes, they are primarily

oxygen; at intermediate altitudes, helium; and at very high altitudes, hydrogen. The boundary heights and the densities vary in a complicated manner with the time of day, time of year, and solar activity (ref. 13). However, for all conditions of interest the densities are sufficiently low that free-molecule flow prevails. The most probable velocities of the particles are indicated in a relative manner on figure 1 by the lengths of the arrows. The average random thermal velocities of oxygen and helium ions and atoms are much less than satellite velocity and will be neglected in the subsequent analysis. In the region where hydrogen ions and atoms are dominant, thermal velocity is comparable to satellite velocity and thus cannot be neglected. For this reason the subsequent theoretical analysis will be applicable only to altitudes below the hydrogen band. The electron thermal velocity is directed along helical paths about the earth's magnetic lines and is much larger than satellite velocity.

Because the electron velocity is much higher than the ion velocity, a net negative current will flow initially from the ambient atmosphere to an uncharged satellite. The flow will continue until the satellite accumulates an equilibrium charge sufficiently negative to repel enough low-energy electrons that the total electron flux to the satellite surface just equals the ion flux to the surface. The equilibrium condition is altered somewhat by photoejection of electrons by solar radiation and possibly by antenna systems which may locally energize electrons to allow them to proceed to the surface against larger negative potentials. For the purposes of the present report, no attempt will be made to estimate the satellite potential (this has been done in refs. 6 and 9), but rather a negative potential will be assumed to exist. The authors of references 1 and 2 report, from actual measurements aboard satellites, potentials of -0.15 and -4 volts, respectively.

To define explicitly the term electric drag, particle trajectories relative to the satellite are shown in idealized form in figure 2 for both a charged and an uncharged satellite. For the uncharged satellite shown in figure 2(a), both the ions and atoms appear to stream along straight, parallel lines as the satellite sweeps them up. Thus, the drag is influenced only by impact and reflection of the particles within a cross section having the same diameter as the body. If the satellite acquires a negative potential as shown in figure 2(b), the ions are deflected toward its surface as they come within the region of influence of this potential. Now the effective cross section for ion collisions is increased as indicated, and the drag of the satellite is increased. Other ions that are deflected but do not impact also cause drag on the satellite through momentum transfer. A third factor that can increase the drag concerns the impacting ions that now strike the surface with more momentum because they have been accelerated by the surface potential. This increase in ion momentum does not directly affect the drag upon impact because it is exactly counteracted by the momentum acquired by the satellite upon accelerating the ions. However, any ions which rebound do so (as neutral particles) with a momentum proportional to the increased impacting momentum, and a net drag increment can result. The difference in drag between (a) and (b) in figure 2 which includes all three of these effects is herein defined to be the electric drag.

Electric-Drag Theories

General review.- The complexity of the electric-drag problem has led all authors of electric-drag theories to make some rather gross assumptions in the formulation of their theories. Because it is not possible to obtain closed-form solutions if the ion-surface collisions are considered in detail, some authors have chosen to circumvent this aspect of the problem. Chopra (ref. 4), for example, has chosen to regard the satellite as a "test particle" that passes through a field of atmospheric ions and scatters them without direct surface collisions. Even though the surface collisions are neglected, the Chopra theory generally gives the highest estimates of electric drag as shown in figure 3. The high drag values result from the fact that the Chopra theory does not allow for shielding of ions from the satellite charge by ambient electrons. Thus the satellite potential is effective over a long range. Wyatt (ref. 5) also circumvents the surface collision problem although he allows for shielding effects. Wyatt assumes the body to be completely permeable to both ions and electrons. The result both of neglecting hard collisions of ions with the surface and of limiting the extent of the satellite potential field by shielding is to estimate a negligible electric drag. Jastrow and Pearse (ref. 3) were the first to account for the details of the ion-surface collisions. Since the Jastrow-Pearse theory was found to agree substantially with the present experimental results, it will be discussed in some detail in the following section.

Jastrow-Pearse theory.- The theoretical model for the Jastrow-Pearse theory is shown in sketch (a). The satellite is assumed to be charged negatively. The negative charge repels all but the highest energy electrons so that a sheath region deficient in electrons is formed about the surface. The sheath is assumed to be spherically symmetric for mathematical simplicity. In reality, the high velocity of the satellite distorts the sheath somewhat on the front side and creates a wake deficient in ions at the rear. A further assumption is that the ion density is constant throughout the sheath and equal to the ambient ion density. Far from the satellite, the electron density is equal to the ion density, and in the sheath the electron density is assumed to adjust itself according to the Boltzmann distribution.

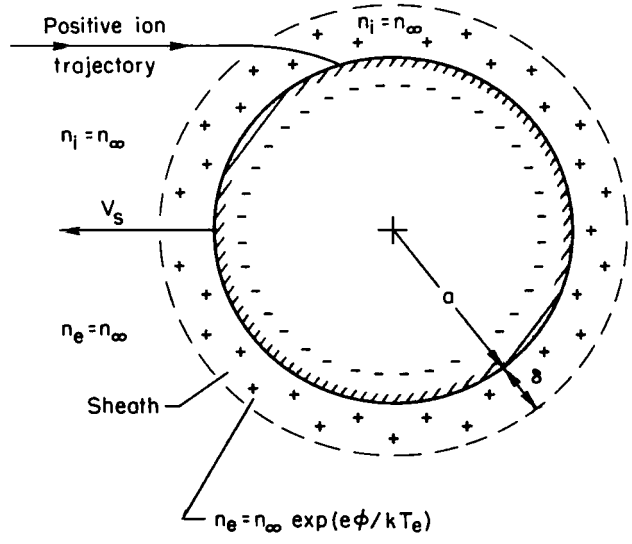

Sketch (a)

$$n_e = n_\infty \exp(e\varphi/kT_e)$$

Evaluation of electric drag by the Jastrow-Pearse theory is carried out in three steps. First, the potential variation through the sheath region is evaluated. The movement of ions through the sheath is not considered since the assumption of constant ion density implies that ion motion has no effect on the potential field. The second step is to compute numerically a network of ion trajectories through the potential field obtained from the first step. This establishes the ion flux and angle of incidence at each point on the satellite surface. Finally, the momentum transfer, and hence the drag, is computed from known, or assumed, reflection characteristics at the surface. The drag due to the scattering of ions that do not strike the surface is also evaluated and can be the dominant electric-drag effect for bodies small enough that the sheath thickness δ is large compared to the radius a.

The potential is determined from Poisson's equation,

$$\nabla^2\varphi = -4\pi\rho \tag{1}$$

where ρ, the charge density, is given by the following equation:

$$\begin{aligned}\rho &= e(n_i - n_e) \\ &= en_\infty[1 - \exp(e\varphi/kT_e)]\end{aligned} \tag{2}$$

When equations (1) and (2) are combined, Poisson's equation becomes

$$\nabla^2\varphi = -4\pi n_\infty e[1 - \exp(e\varphi/kT_e)] \tag{3}$$

Introducing the dimensionless variables Φ and R, defined as

$$\Phi = (r/\lambda_D)(e\varphi/kT_e) \tag{4a}$$

and

$$R = (r/\lambda_D) \tag{4b}$$

where

$$\lambda_D = \sqrt{kT_e/4\pi ne^2}$$

yields the following dimensionless differential equation:

$$\frac{d^2\Phi}{dR^2} = R[\exp(\Phi/R) - 1] \tag{5}$$

Equation (5) was solved numerically on the IBM 7090 computer with the following boundary conditions:

$$\varphi = \varphi_o \quad \text{at} \quad r = a$$

and

$$\varphi = 0 \quad \text{at} \quad r = \infty$$

Once the potential distribution has been determined, the trajectories of individual ions are obtained by integration of the force equation, $F = -e\nabla\varphi$, through the sheath (see, e.g., ref. 14). Figure 4 shows a typical set of trajectories.

The final step in the drag estimation is to compute the momentum transfer rate from both those ions which impact with the surface and those ions which are deflected around the surface. The drag due to the nonimpacting ions is easily computed from the momentum change of the ions in the drag direction as they are deflected in passing the sphere. Schamberg (ref. 15) treats the ion impact reaction in detail. In the hard collision process, the impact and the reflection can be considered as two separate steps. Each ion, upon impact with the surface, exchanges the relative free-stream momentum, mv_s, with the satellite regardless of the impact point on the surface. The momentum imparted to the satellite by reflection depends on the impact point, the angle of incidence, the type of reflection, the degree of momentum accommodation, and whether the incident ion reflects as an ion or as a neutral. It is generally believed that the ions are neutralized on impact so that they will probably be reflected as neutral atoms. The point of impact and the angle of incidence are known from the trajectory calculations. However, the type of reflection and the degree of momentum accommodation are not generally predictable. Hurlbut (ref. 16) and Wachman (ref. 17) give good summaries of the current state-of-the-art on accommodation coefficients. The reflection problem is further complicated by the existence of sputtered particles. Wehner (ref. 18) shows that the contribution of sputtered particles to the drag can exceed the contribution of reflected ions. In lieu of reliable information on momentum accommodation and on the type of reflection, the assumption is made that the ion momentum is absorbed without reflection, or is fully accommodated to a cold surface, a condition herein referred to as full momentum accommodation. The experimental results presented in references 18 and 19 indicate that such an assumption is reasonable for the model surfaces of the present investigation. For fully accommodating surfaces, the ratio of the impacting ion drag of a charged sphere to that of an uncharged sphere is simply

$$\frac{D}{D_O} = \frac{D_O + D_E}{D_O} = \left(\frac{p_g}{a}\right)^2 \tag{6}$$

where p_g is the grazing impact parameter, or effective cross-section radius (fig. 2(b)).

Extensions have been made to the Jastrow-Pearse theory by Hohl and Wood (ref. 6) and by Davis and Harris (ref. 7). The major contribution in the Hohl and Wood paper is the inclusion of the effect of the earth's magnetic field on satellite drag. Also, in this paper the Boltzmann distribution for the electron number density in the sheath is modified to account for the fact that electrons are probably absorbed by the surface on impact. This can be an important correction when the parameter $(-e\varphi_O/kT_e)$ is of the order 1 or less,

but the correction is small when this parameter is large, as it was for the conditions of the present experimental investigation. Since for the present program the electron absorption effect is expected to be small and the magnetic field is negligibly small, the Jastrow-Pearse theory and the Hohl-Wood theory should agree very closely. In reference 7 the assumption of constant ion density is relaxed by an iterative procedure by which the ion density approaches its proper distribution.

Scaling Relations

As is usually the case, it was not possible in this investigation to duplicate in the laboratory the exact conditions encountered by satellites in space. The relationships between probable space conditions and those in the present experimental investigation are shown in the following list:

Parameter	Space	Laboratory
Ion species	He^+ or O^+	Hg^+
Ion density	$\leq 10^6$ cm^{-3}	10^8 cm^{-3}
Ion energy (relative to surface)	1 to 5 ev	100 to 250 ev
Ion velocity	8×10^5 cm/sec	1.0 to 1.6×10^6 cm/sec
Electron thermal energy	0.2 ev	2 to 3 ev
Mean-free path	10^7 to 10^{10} cm	50 cm
Debye radius	Order of cm	0.10 to 0.13 cm
Body diameter	Order of meters	1.9 to 2.5 cm
Surface potential	-4 to -0.1 volts	-250 to 0 volts

Because such large differences exist between laboratory and space conditions, scaling rules are necessary for the laboratory results to be meaningful. As will now be shown, the Jastrow-Pearse theory allows for the easy development of such rules.

Since, in the Jastrow-Pearse theory, the potential field is calculated independently of the ion motion, the scaling of the potential distribution can also be done independently of the scaling of the ion trajectories. Scaling parameters for the potential can be obtained from equation (5). This

second-order equation will have a solution of the form

$$\Phi = f(R;C_1,C_2) \tag{7}$$

where C_1 and C_2 are constants that depend on the boundary conditions

$$\Phi = \Phi_o \quad \text{at} \quad R = R_o$$

$$\Phi = 0 \quad \text{at} \quad R = \infty$$

The dimensionless parameter Φ (as defined by eq. 4(a)) will approach zero as the radial distance approaches infinity because the potential, φ, approaches zero more rapidly than $1/r$, as is the case for any shielded potential. Hence, the boundary condition at infinity is satisfied for spheres both in space and in the laboratory, and the constants C_1 and C_2 depend only on the surface parameters Φ_o and R_o. Equation (7) can then be written

$$\Phi = f(R;\Phi_o,R_o)$$

and the potential distribution around any two spheres is geometrically similar, provided Φ_o and R_o are identical. The quantities Φ_o and R_o are, therefore, scaling parameters as are any two combinations of these parameters. We choose to take $R_o = a/\lambda_D$ and $\Phi_o/R_o = e\varphi_o/kT_e$ as the scaling parameters since these forms have simple physical interpretations. The first parameter relates a characteristic length of the sphere, namely its radius, to the Debye radius, λ_D, which is a characteristic length of the plasma. The second parameter is the ratio of the sphere surface potential to the average thermal energy of the electrons. Since electrons are repelled by the surface potential, this parameter determines the depth of penetration of the average electron into the sheath.

The scaling parameter for the ion-trajectory calculation comes directly from the Lagrangian equations of motion for a charged particle in a spherically symmetric potential field. From reference 14 one finds, after the first integration,

$$\frac{d\theta}{d\,\frac{r}{a}} = \frac{\frac{p}{a}}{\frac{r^2}{a^2}\left[1 - \frac{p^2/a^2}{r^2/a^2} - \left(\frac{a}{r}\right)\left(\frac{\Phi}{\Phi_o}\right)\left(\frac{e\Phi_o}{E}\right)\right]^{1/2}} \tag{8}$$

Since Φ is already scaled, equation (8) provides scaling in units of body radii, provided $e\varphi_o/E$ is fixed in both systems. Thus, for two systems to be comparable it is necessary that Φ_o, R_o, and $e\varphi_o/E$ all be the same in both systems.

An example of comparable conditions in space and in the laboratory is shown in the following list for a satellite at 1000 km in an O^+ atmosphere:

	a, cm	φ_o, volt	E, ev	n_e, cm^{-3}	kT_e, ev	λ_D, c	R_o	$\frac{\Phi_o}{R_o}$	$\frac{e\varphi_o}{E}$
Lab	1.3	-60	60	10^8	3	0.13	10	-2.0	-1
Space	26	-5	5	2×10^4	0.25	2.6	10	-2.0	-1

The three parameters scale the behavior of the ions to the point of impact with the satellite surface. Up to that point the fact that the laboratory system contains Hg^+ and the space system some other ion is not important in the Jastrow-Pearse theory, provided the scaling parameters are the same in both systems. The momentum transfer does depend on the ion-surface system, but the system becomes unimportant when the assumption is made that the ion momentum is completely absorbed, since then the drag depends only on the impact parameter p_g of the grazing ions (eq. (6)).

APPARATUS AND PROCEDURES

Plasma Apparatus

The plasma apparatus (figs. 5, 6, and 7) provides a singly ionized mercury plasma that is directed toward the model at an energy variable between about 60 and 250 ev. At 65 ev the velocity of mercury ions is 8×10^5 cm/sec, or about earth satellite velocity. The density of the streaming beam is 10^8 ions/cm^3. The background mercury pressure is regulated by pumping and by cooling with a Freon 12 refrigeration system to keep the mean-free path about 50 cm so that the models are in free-molecule flow.

The discharge is started by a high-voltage pulse to the igniter (see fig. 5). The arc is sustained by the auxiliary anode which operates about 12 volts positive with respect to the grounded mercury pool. Electrons from the arc are accelerated toward the main anode which normally operates about 27 volts positive. Since the electron energy is near the optimum for singly ionizing mercury but below the second ionization potential, a thermal plasma of singly ionized mercury ions is formed. The mesh is operated at a negative potential which depends on the ion energy desired. The negative potential accelerates the ions but retards the electrons so that an electron-deficient sheath is formed. The mesh openings are small compared to the sheath thickness so that the sheath boundary is essentially planar and the ions are accelerated parallel to the axis. Upstream of the mesh the plasma floats at nearly the main anode potential so that the difference between main anode and mesh potentials determines the energy of the ions. To minimize beam divergence due to mutual repulsion of the ions, electrons are introduced into the stream from a tungsten wire emitter just downstream of the mesh.

It was discovered from force measurement results that a significant portion of the force on models in this system was due to a component of high velocity neutral atoms in the beam. To correct for this neutral component a set of ion deflectors was introduced which could be charged electrically to filter out the ion and electron component. Then the force due to the neutral component could be measured and applied as a tare correction to the total force to obtain the forces due to ions. The ion deflectors consist of thin strips of steel shimstock, 2 cm wide and spaced 0.6 cm apart. When the deflectors are uncharged, all elements are connected to the mesh to create minimum effect on the plasma flow. When the deflectors are charged, alternate elements are at -150 volts with respect to the other half of the elements which are at mesh potential. The resulting potential gradient deflects the charged particles and reduces the ion current detected by probes at the model position to less than 5 percent of that detected when the deflectors are uncharged. To determine the effect of the ion deflectors on the plasma, measurements were made, with the deflectors both charged and uncharged, of the ion current to a Langmuir probe placed in the plasma immediately upstream of the deflectors. No significant differences were noted. This behavior would be expected, since a plasma generally assumes the most positive boundary potential, and since the most positive boundary was maintained at mesh potential for both the charged and uncharged modes of ion deflector operation.

Plasma Surveys

The plasma beam was surveyed with two instruments. The relative density distributions in the beam were studied with Langmuir probes. The energy spectrum of the ions and also the relative density distributions were determined by a Faraday cage (fig. 8). The grid is operated at a negative potential to repel the electrons and the plate is operated at a variable positive potential with respect to the mesh. The energy spectrum of the ion beam is determined from the curve of plate current versus retarding potential. Typical curves are shown in figure 9 for mesh accelerating voltages of 120 and 210. The curves are fairly flat over the lower voltage range because most of the ions are sufficiently energetic to overcome these retarding potentials. At higher voltages the current falls off rapidly to zero at retarding potentials that exceed the energy of the most energetic ions. The voltage for half-maximum current indicated on the curves is taken as the average energy of the ions. Figure 10 shows the radial variation of the average ion energy as determined from curves similar to those of figure 9. Radial ion density surveys are shown in figure 11. The data are normalized by the density at the center of the test section. The indicated core diameter, which is about twice the maximum model diameter, is defined as the diameter of the cylindrical section of the beam within which the density differs from the average density by less than ±5 percent.

The average ion density at the model is obtained from measurements with the movable concentric ring disk shown in figure 12. The disk was made by cementing an aluminum foil to an insulating background and scribing a thin circular cut in the foil to separate the two segments electrically. Separate

conductors connected both inner and outer surfaces to a common power supply, but only the current from the center disk was measured. This arrangement allowed current collection without edge effects. The characteristic curve for the center element of the disk probe is shown in figure 12(b). As the disk potential is reduced from 0 to -50 volts more and more of the electrons are repelled. Between -50 and -150 volts the disk current is insensitive to disk potential, a result indicative of nearly one-dimensional flow to the center disk. Finally, for potentials below -150 volts the current begins to increase as the edge effect spills over to the center disk. In a manner consistent with Langmuir probe techniques, the ion current to the disk for the undisturbed plasma is taken as the linear extrapolation to zero potential of the one-dimensional portion of the characteristic curve. Then the average ion number density is given by the relation

$$n_i = \frac{i}{ev_iA}$$

where A is the area of the center disk, i the measured ion current, and v_i the ion velocity as determined from Faraday cage characteristic curves.

Microbalance

Drag of the spherical models was measured by means of the quartz-fiber torsion microbalance shown in figure 13. Primary design requirements were that the balance be capable of (1) supporting a 2-gram model, (2) remotely measuring drag forces in the vacuum test chamber from zero to several milligrams, and (3) providing an electrical connection for maintaining a potential on the model surface.

The torsion element was a quartz fiber about 0.006 cm in diameter and 18 cm long which was fused to larger quartz members at each end. The upper end was fastened within a steel shaft which passed through an O-ring seal in the supporting top plate and was connected by a 120:1 gear train to a manually turned counter. The lower end of the torsion fiber was fused to a balance crossarm assembly made of 1-mm-diameter quartz rod. Two diametrically opposed crossarms had bayonet type electrical connectors for attaching the model and counterweight. An insulated electrical lead was brought from the model connector to the center of the balance arm, from which a finer wire led to a vacuum-sealed connector through the upper vacuum plate. Extraneous torque due to stiffness of this wire was made negligible by employing a slack tungsten wire 0.0004 cm in diameter and several centimeters long to make the connection upward from the center of the balance arm.

From the vertical rod below the crossarm assembly, a horizontal wire wheel was suspended into a small pan of diffusion-pump oil to provide the required damping of torsional oscillations during drag measurements. The stainless steel balance frame, attached to the steel top plate, supported the oil damper pan and two worm-and-screw mechanisms for caging the crossarms when the balance was adjusted or models changed. A shield (not shown in fig. 13) extending from the frame protected the balance arm from aerodynamic

tare forces, although generally these tares were small compared with the model drag. Drag readings were made with the balance installed in such a position that the plane through the model center and the torsion fiber was normal to the axis of the plasma stream. To null the balance, the upper end of the quartz fiber was turned by the geared external counter until a reference point on the counterweight made small oscillations centered on a vertical hairline.

The microbalance was calibrated to relate increments in counter reading to increments in drag force. The calibration was first made by a gravity-loading method, with the torsion fiber held in tension by a lower quartz fiber of 0.0025-cm diameter which permitted the empty balance to be turned with the torsion fiber horizontal. With the balance arm in a horizontal position, the balance was nulled using the filar microscope and the counter reading was recorded. This procedure was repeated for each of several known weights applied at a known radius, and the resulting calibration curve was found to be linear over the entire range of ±3 milligrams. The lower fiber had much less torsional stiffness than the upper fiber and was returned to its initial position and torque at each null reading, hence did not contribute any torque to the calibration. From this basic determination of torsion-fiber stiffness, the calibration of counter reading against drag in micrograms could be calculated for any model lever arm.

A second calibration method was developed which made use of the simple harmonic motion of the balance swinging undamped from the upper torsion fiber. For the balance beam making small torsional oscillations, the deflection, α, per unit torque is related to the period, P_1, and the moment of inertia, I_1, in the following manner:

$$\frac{\alpha}{T_q} = \frac{P_1^2}{4\pi^2 I_1} \tag{9}$$

The value of I_1 is only known approximately, but if the moment of inertia is increased by a known amount, this difficulty can be circumvented. Adding a small mass, m_2, symmetrically (near the model and counterweight positions) at a known lever arm, l, increases the moment of inertia to

$$I_2 = I_1 + 2m_2 l^2 \tag{10}$$

In the increased period of oscillation, P_2, the same deflection per unit torque is now

$$\frac{\alpha}{T_q} = \frac{P_2^2}{4\pi^2(I_1 + 2m_2 l^2)} \tag{11}$$

Use of equations (9) and (11) gives the result in easily measured quantities as

$$\frac{\alpha}{T_q} = \frac{P_2^2 - P_1^2}{8\pi^2 m_2 l^2} \tag{12}$$

From this value of α/T_q the balance counter reading is easily related to force on any model, when the model's effective lever arm and the counter gear ratio are known. The balance calibration obtained by the swing-period method checked within ±1-1/2 percent with that obtained by the dead-weight method and, because of its greater convenience, the swing method was employed for the periodic calibrations throughout the tests. The calibrations were considered to be repeatable within ±2 percent, and the best precision of an individual drag reading was about 2 micrograms.

Models

The measurements and the experimental facilities required that the models be spherical, have a diameter less than 3 cm, weigh less than 2 grams, have a conducting surface, and be easily connected mechanically and electrically to the balance. These requirements were met by models constructed from hollow spheres of glass. A gold film was vacuum deposited on the surface and made electrical contact with a connector fixed to the model. Sliding this connector onto the matching connector on the balance crossarm therefore served both to support the model and to make the electrical contact required to control the surface potential externally. This support was made small in comparison to the model size to minimize interaction with the wake. Spherical models of 1.9- and 2.5-cm diameter were employed, each having a matching cylindrical brass counterweight.

Experimental Procedure

Measurements were made of the drag on spherical models as the model potential relative to the plasma was varied. For convenience, the surface potential was actually referred to the mesh potential, inasmuch as the plasma potential differed only a few percent from the mesh potential so that reference to mesh potential rather than plasma potential created only a small error.

The total drag measured consisted of the drag due to the neutral atoms as well as the drag of the ions. The neutral drag component was determined and applied as a tare correction as described in the section on plasma apparatus. A typical test procedure is as follows: (1) The ion deflectors were charged so that only the neutral flow reached the models, and the balance was nulled. (2) With the model at zero potential, the charge was removed from the deflectors to allow the ions to also reach the model, and the balance was again nulled. The increment in force is the zero-charge ion drag. (3) The model potential was increased in steps and the balance was nulled at each step. The electric drag was obtained as the difference between the measurements with the model charged and the model uncharged. This technique of using the difference between two measurements minimized errors due to a small, constant radiometer force on the models. To assure the constancy of the

radiometer force, the equipment was allowed to operate for about an hour prior to each run so that the system could approach thermal equilibrium.

To check for possible errors due to static attraction effects, electric potentials were applied between the model and the balance frame with the discharge off but with the test section under vacuum. No significant forces were observed until potentials greater than those used in the test were applied. With the plasma flowing, the effect of static fields should have been even less, since a plasma forms sheaths that tend to shield any static charges.

The range of variables covered was dictated by the plasma beam characteristics and the capability of the balance. It was desirable to have the models as large as possible, both to decrease the ratio of support tare to model drag and to produce forces that were large enough to measure accurately. The balance load capability and the usable plasma-beam diameter limited the maximum diameter. Model diameters of 2.5 and 1.9 cm were chosen as reasonable compromises. The ion energy range of 60 to 250 electron volts was dictated by the capability of the plasma apparatus. The model potentials were then determined by the scaling requirement that $e\varphi_o/E$ be fixed. Assuming values of $e\varphi_o/E$ between -1 and 0 for the satellite condition resulted in laboratory values between -250 and 0 volts for φ_o. With such large magnitudes for φ_o together with electron thermal energies of the order of 1 to 3 ev, the magnitude of the scaling parameter, $e\varphi_o/kT_e$, is much greater than unity. Values greater than unity are realistic for satellite conditions for which electric drag is likely to be large.

RESULTS AND DISCUSSION

For the purpose of interpreting the results of this investigation, it has been assumed that all the momentum of the ions is absorbed by the model surfaces on impact. For extremely clean surfaces, this would not necessarily be a good assumption (ref. 17), but for the practical surfaces used in the present investigation, the assumption is reasonable (see fig. 14). Data are presented for the drag on a flat plate due to the normal impingement of mercury ions. The ordinate is the total measured drag due to both impact, D_I, and recoil, D_R, compared to an impact-only drag computed from the known ion flux to the target. Calculated values of $(D_I + D_R)/D_I$ are presented for both full momentum accommodation ($D_R = 0$) and zero accommodation. The experimental drag differs from that of the complete momentum accommodation condition by, at most, 15 percent. Results of reference 18 indicate that the recoil drag component, D_R, is primarily due to sputtering of surface material rather than reflection of incident particles.

Data for the drag of uncharged spheres are presented in figure 15. Again it is apparent that the data are generally within 15 to 20 percent of the complete momentum accommodation condition, $D_R = 0$. Because the primary purpose of this investigation was to resolve order-of-magnitude differences in published electric drag theories, a 15-percent error due to assuming complete accommodation for estimation purposes is not considered significant. An

interesting observation to be made from figure 15 is that the drag of the uncharged sphere is less than that for complete accommodation. As indicated by the cross-hatched region, the drag should be greater than or equal to the complete accommodation value for any form of uniform reflection over the entire surface, ranging from specular to diffuse and from zero to full accommodation. It is possible for the sphere drag to be less than the complete accommodation value if the reflection characteristics are not uniform over the entire surface. An extreme example is shown by the inset (fig. 15). The situation shown is designed to give the minimum possible drag for an uncharged sphere and serves to establish the lower limit on $(D_I + D_R)/D_I$. Complete accommodation is assumed for the ions that impinge on the inner region where any type of reflection would contribute a positive drag. Specular reflection with zero accommodation, hence maximum magnitude of D_R, is assumed for the outer region where specular reflection would contribute a negative force. Although such a severe variation of reflection characteristics is not to be expected physically, it appears from the data that a tendency exists toward more specular reflection from the region of the frontal surface where the ion incidence angle is more than 45° from the normal to the surface.

The results of the electric-drag measurements are presented in figures 16(a) and 16(b), as the variation of ion drag ratio, D/D_o, with energy ratio, $-e\varphi_o/E$. The electric drag caused by the surface charge is seen to be substantial, causing the ion drag to approximately double when the energy ratio is increased from zero to unity. Of the three theories (shown in fig. 3) only that of Jastrow and Pearse agrees reasonably with the data and is presented for comparison. The theoretical curves shown on figure 16 result from calculations both for the case that considers only ion impacts and the case that considers both ion-impact and ion-scattering contributions. These are shown on figure 16 for the two values of a/λ_D corresponding to the two model sizes used. The addition of nonimpact ion scattering greatly improves the agreement (to within 10 percent) between experiment and theory for the smaller sphere ($a/\lambda_D = 7.5$). It is apparent that test conditions are such as to place the two models about on the border where the nonimpact drag effects become significant. The much greater effect for the smaller sphere is consistent with a previous statement that nonimpact scattering can become a dominant effect on the drag of spheres as the relative sheath thickness, δ/a, becomes large.

Of the three scaling parameters developed in the theoretical considerations section, it was possible to verify experimentally the correlation of only the energy-ratio parameter, $-e\varphi_o/E$. Figure 16 shows that the data are correlated within experimental scatter by this parameter for ion energies between 100 and 200 electron volts. The effectiveness of the other parameters, $e\varphi_o/kT_e$ and a/λ_D, for correlating the data could not be examined experimentally because electron temperature and number density could not be regulated.

The data of figure 16 can be related to particular satellite conditions by the scaling parameters. For example, for $-e\varphi_o/E = 1$, the laboratory model having $a/\lambda_D = 10$ corresponds to a 52-cm-diameter satellite at about 1000 km altitude. For $-e\varphi_o/E = 1$, the satellite potential would be -5 volts for an

O^+ atmosphere or -1.25 volts for a He^+ atmosphere. According to reference 12, the atmosphere may be either predominantly oxygen or predominantly helium, depending upon the time of day. Potential measurements aboard satellites have ranged from -4 to -0.15 volts.

To evaluate the importance of electric drag on satellites from the results of this investigation, the present results, which are for a fully ionized plasma, must be modified to the partially ionized plasma of the earth's upper atmosphere. With the assumption of a single species of atom and ion this modification is accomplished by the following equation:

$$\frac{D}{D_O + D_n} = \left(\frac{D}{D_O}\right)\left(\frac{n^+}{n^+ + n_N}\right) \tag{13}$$

where subscript N denotes neutral particles. It is apparent from equation (13) that the importance of electric drag is directly dependent on the percentage ionization of the atmosphere. The magnitude of the percentage ionization in the atmosphere has not been reliably established as yet, but it tends to increase with increasing altitude.

Because the experimental values of electric drag agreed quite well with the Jastrow-Pearse theory, it appeared possible that systematic use of the machine solutions might permit formulation of an approximate equation relating the electric drag of spheres to the scaling parameters. Such an equation would be much more convenient than the machine results and might provide the required accuracy for most engineering purposes.

As noted in previous sections, the three useful similarity or scaling parameters were a/λ_D, $-e\varphi_O/E$, and $-e\varphi_O/kT_e$. These parameters, or equivalent combinations, are necessary for fully scaling both the potential field about the charged body and the ion trajectories through the potential field.

Values of D/D_O, the ratio of drag of the charged body to that of the uncharged body, generally were approximated for both the experimental and the corresponding machine-calculated results by the relation

$$\frac{D}{D_O} = 1 - \frac{e\varphi_O}{E} \tag{14}$$

Both classical scattering theory and the machine calculations using Jastrow's electric-drag theory indicate that equation (14) defines the upper limit for the drag of impacting particles when the relative thickness of the ion sheath δ/a is sufficiently large that the potential field may be regarded as essentially unshielded. For progressively smaller relative sheath thicknesses, D/D_O might reasonably be expected to decrease toward unity as

$$\frac{D}{D_O} = 1 - \frac{e\varphi_O}{E}\left\{1 - \exp\left[-(F)\left(\frac{\delta}{a}\right)^{\beta}\right]\right\} \tag{15}$$

where F and β are empirical constants or functions of the scaling parameters.

It is possible to relate δ/a to the scaling parameters by the closed-form solution mentioned in reference 3 for the electric potential in a finite spherical sheath. Upon carrying out this solution with the assumption that no electrons penetrate the sheath and that the negative surface charge is exactly balanced by the positive ion charges in a sheath of finite thickness, δ, an implicit equation for δ/a is obtained as

$$\left(\frac{\delta}{a}\right)^2\left(1 + \frac{2}{3}\frac{\delta}{a}\right) = \frac{-e\varphi_o}{2\pi mea^2} \tag{16}$$

using any consistent units. When equation (16) is plotted logarithmically, the value of δ/a is given very well over a range from $0.01 \leq \delta/a \leq 1.0$ by the relation

$$\frac{\delta}{a} = 610\left(\frac{na^2}{-e\varphi_o}\right)^{-0.47} \tag{17}$$

where $-e\varphi_o$ is in electron volts and na^2 is in cm^{-1}. Interestingly, the parameter $(na^2/-e\varphi_o)$ is proportional to $(a/\lambda_D)^2/(-e\varphi_o/kT_e)$, two of the scaling parameters previously derived. Over practical ranges of all the scaling parameters, sample machine computations showed the effects of variations in $-e\varphi_o/kT_e$ and a/λ_D to be small when the variations were such that $(na^2/-e\varphi_o)$ and $(-e\varphi_o/E)$ were held constant. For practical purposes then, electric drag was reduced to a function of the two parameters $(-e\varphi_o/E)$ and $(na^2/-e\varphi_o)$. Machine calculations of electric drag were carried out for several selected values of each at a fixed value of $(-e\varphi_o/kT_e)$. Analysis of the results indicated that over practical ranges, the empirical factor F in equation (15) had a value of $F = 3(-e\varphi_o/E)^{-1.0}$ and the index had the value $\beta = 1.06$. A suitable approximate equation for impact drag over the ranges $0 \leq -e\varphi_o/E \leq 1$ and $0 \leq \delta/a \leq 1$ then is

$$\frac{D}{D_o} = 1 - \left(\frac{e\varphi_o}{E}\right)\left\{1 - \exp\left[-2700\left(\frac{-e\varphi_o}{E}\right)^{-1}\left(\frac{na^2}{-e\varphi_o}\right)^{-1/2}\right]\right\} \tag{18}$$

The variations of drag ratio, D/D_o, with energy ratio $(-e\varphi_o/E)$ given by equation (18) are shown graphically in figure 17 for several values of $(na^2/-e\varphi_o)$ together with the machine-calculated points. Also shown are the calculated values of δ/a corresponding to each value of the parameter $(na^2/-e\varphi_o)$. As the value of δ/a increases toward unity, the drag ratio for impacting ions approaches the limiting value given by equation (14). Marks also indicate on the same vertical scale the values of $(1 + \delta/a)^2$, representing the upper limit of impacting ion drag imposed by the finite sheath when the magnitude of $(-e\varphi_o/E)$ is sufficiently large that all ions entering the sheath impact upon the sphere. The values of $(1 + \delta/a)^2$ calculated by the simple sheath theory agree well with the asymptotic results, for large $(-e\varphi_o/E)$, of the exact machine computation of the Jastrow-Pearse theory, and one might conclude from this agreement that the simplified closed-form sheath analysis may be satisfactory for some purposes. It is also of interest that

the value of D/D_o as given by equation (18) is almost exactly equal to the value ($D/D_o = 1.10$) found by Hohl and Wood for the model described in reference 6. This agreement is to be expected on the basis of the discussion in the section on electric-drag theories.

CONCLUDING REMARKS

Experimental results of this investigation have shown that electric drag can be a significant fraction of the total drag of a satellite if both the magnitude of the satellite potential and the percentage ionization of the atmosphere are sufficiently large. Electric drag is more likely to be significant for small satellites than for large satellites because of the greater ratio of sheath thickness to satellite radius. The results have also shown that theories must include both direct ion-surface collisions and potential shielding effects to give results that correlate with experiment. The Jastrow-Pearse theory, which considers both of these factors, estimates the present experimental results to within 10 percent.

Scaling parameters developed from the Jastrow-Pearse theory allow the extension of the present experimental results to satellite conditions. For example, proper selection of ion energy and surface potential can make the 2.5-cm-diameter sphere in the laboratory equivalent to a 52-cm-diameter satellite at 1000 km altitude. In this example, the effect of surface charge is sufficient to double the ion drag as the ratio of surface electric potential to initial ion kinetic energy is changed from 0 to -1. The scaling parameters and an existing theory are used as guides in developing an approximate equation by which electric drag may be estimated to reasonable accuracy over scaling parameter ranges of practical interest.

Ames Research Center
National Aeronautics and Space Administration
Moffett Field, Calif., Oct. 12, 1964

REFERENCES

1. Bourdeau, R. E., Donley, J. L., Jr., Serbu, G. P., and Whipple, E. C., Jr.: Measurements of Sheath Currents and Equilibrium Potential on the Explorer VIII Satellite (1960 X). NASA TN D-1064, 1961.

2. Whipple, E. C., Jr.: The Ion-Trap Result in Exploration of the Upper Atmosphere With the Help of the Third Soviet Sputnik. NASA TN D-665, 1961.

3. Jastrow, R., and Pearse, C. A.: Atmospheric Drag on the Satellite. J. Geophys. Res., vol. 62, no. 3, Sept. 1957, pp. 413-23.

4. Chopra, K. P.: Interactions of Rapidly Moving Bodies in Terrestrial Atmosphere. Rev. Modern Phys., vol. 33, no. 2, April 1961, pp. 153-89.

5. Wyatt, P. J.: Induction Drag on a Large Negatively Charged Satellite Moving in a Magnetic-Field-Free Ionosphere. J. Geophys. Res., vol. 65, no. 6, June 1960, pp. 1673-8.

6. Hohl, Frank, and Wood, George P.: The Electrostatic and Electromagnetic Drag Forces on a Spherical Satellite in a Rarefied Partially Ionized Atmosphere. Paper presented at the Third International Symposium on Rarefied Gas Dynamics, Paris, France, June 26-30, 1962.

7. Davis, A. H., and Harris, I.: Interaction of a Charged Satellite With the Ionosphere. NASA TN D-704, 1961.

8. Kraus, Lester, and Watson, Kenneth M.: Plasma Motions Induced by Satellites in the Ionosphere. Phys. of Fluids, vol. 1, no. 6, Nov.-Dec. 1958, pp. 480-88.

9. Beard, David B., and Johnson, Francis S.: Charge and Magnetic Field Interaction With Satellites. J. Geophys. Res., vol. 65, no. 1, Jan. 1960, pp. 1-7.

10. Jefimenko, Oleg: Effect of the Earth's Magnetic Field on the Motion of an Artificial Satellite. Amer. Jour. Phys., vol. 27, May 1959, pp. 344-48.

11. Brundin, Clark L.: Effects of Charged Particles on the Motion of an Earth Satellite. AIAA Jour., vol. 1, no. 11, Nov. 1963, pp. 2529-38.

12. Bauer, S. J.: Helium Ion Belt in Upper Atmosphere. Nature, vol. 197, no. 4862, Jan. 5, 1963, pp. 36-7.

13. Harris, Isadore, and Priester, Wolfgang: Theoretical Model for the Solar Cycle Variation of the Upper Atmosphere. NASA TN D-1444, 1962.

14. Goldstein, Herbert, Ph.D.: Classical Mechanics. Addison-Wesley Pub. Co., Reading, Mass., 1950.

15. Schamberg, R.: A New Analytic Representation of Surface Interaction for Hyperthermal Free Molecule Flow With Application to Neutral-Particle Drag Estimates of Satellites. Rand Corp., RM-2313, Jan. 8, 1959.

16. Hurlbut, F. C.: On the Molecular Interactions Between Gases and Solids. Univ. of Calif. Inst. of Eng. Res., TR HE-150-208.

17. Wachman, Harold Y.: The Thermal Accommodation Coefficient: A Critical Survey. Amer. Rocket Soc. Jour., vol. 32, no. 1, Jan. 1962, pp. 2-12.

18. Wehner, Gottfried: Studies of the Interaction of High-Velocity Atoms With Solid Surfaces by Means of Gas Discharge Devices. Project Rand Aerodynamics of the Upper Atmosphere, R-339, June 8-10, 1959.

19. Savage, Howard F., and Bader, Michel: Momentum Accommodation of N^+, N_2^+, and A^+ Incident on Copper and Aluminum from 0.5 to 4 kev. NASA TN D-1976, 1963.

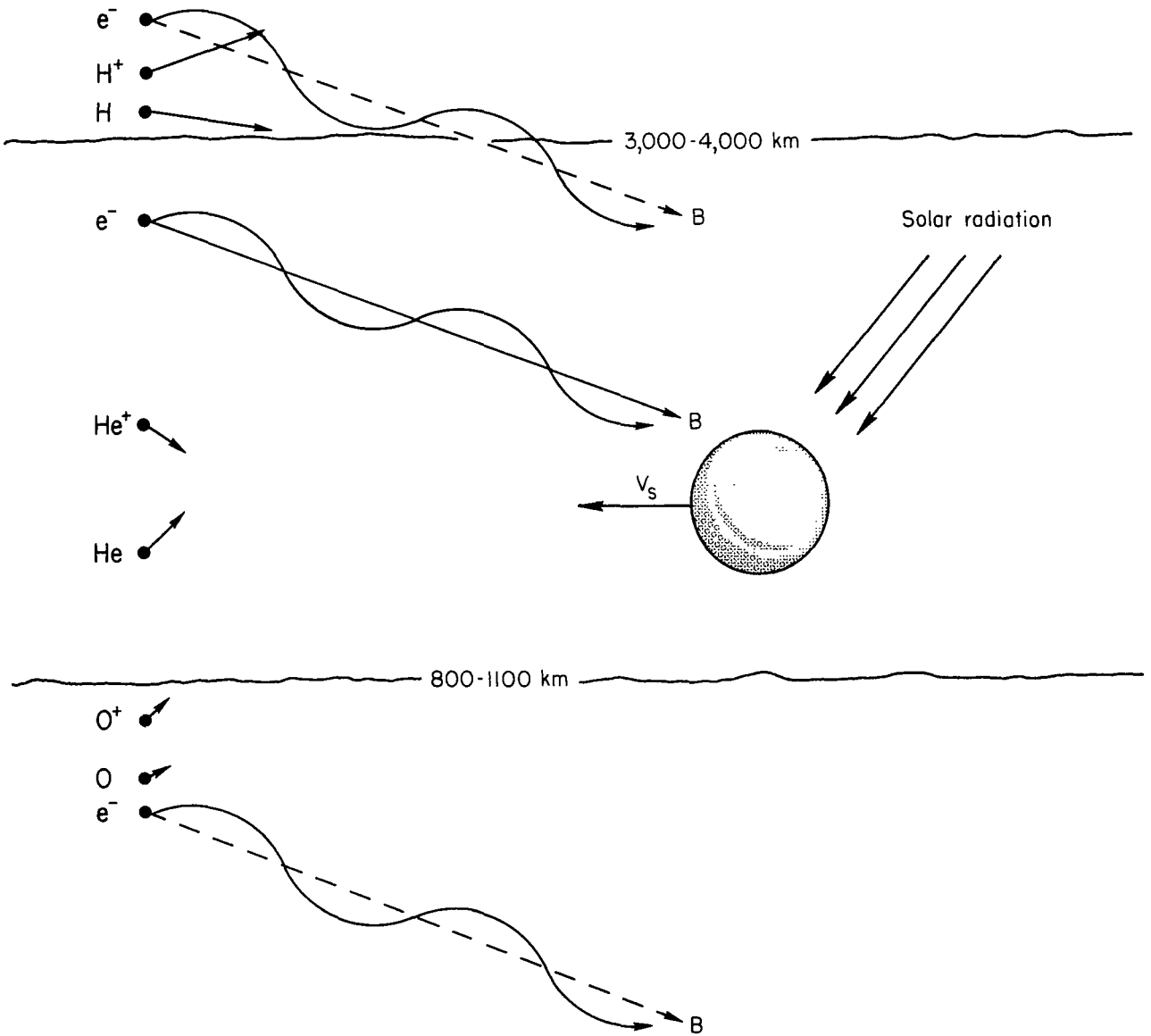

Figure 1.- Conceptual drawing of satellite environment.

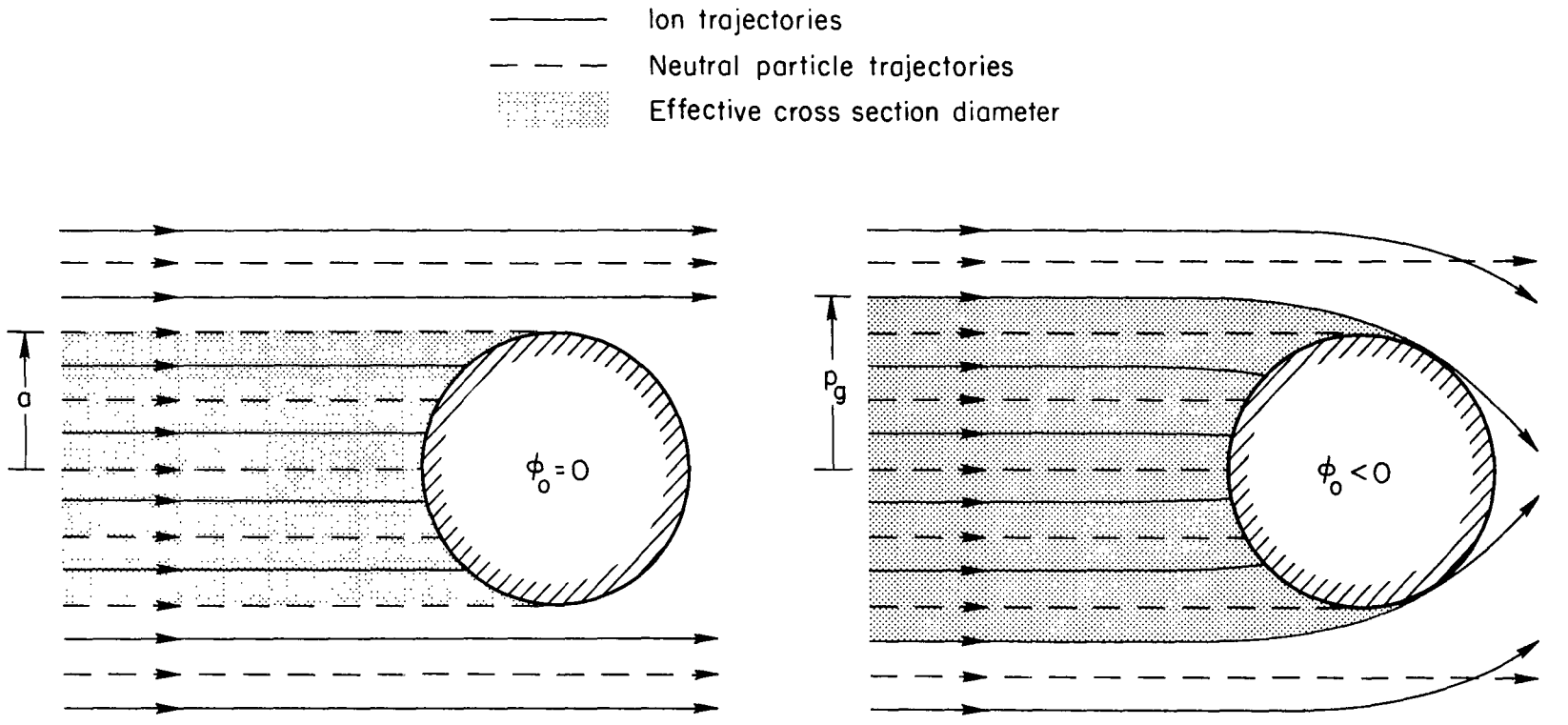

(a) Zero net charge.

(b) Negative net charge.

Figure 2.- Effect of satellite charge on ion trajectories.

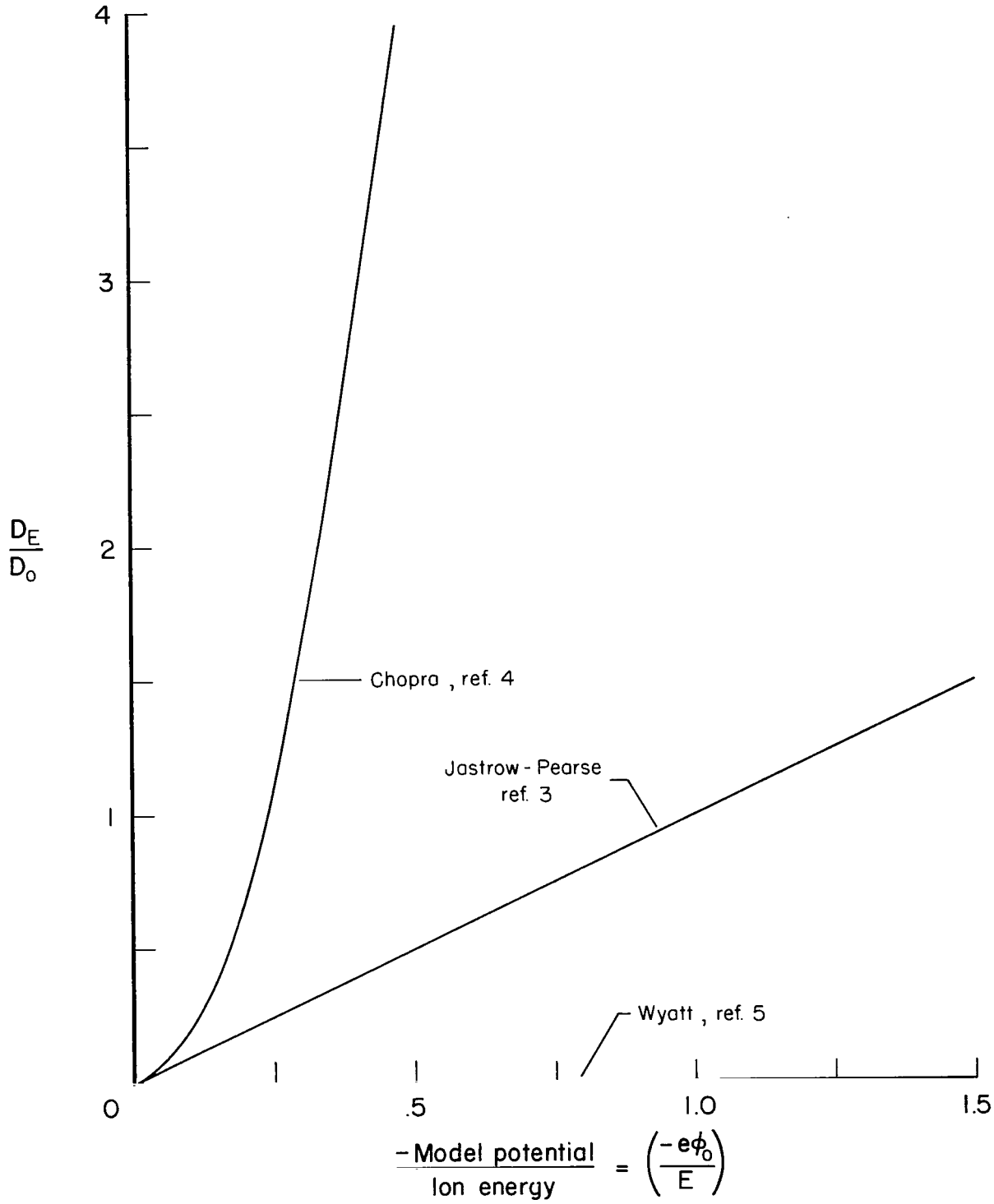

Figure 3.- Comparison of electric-drag theories for a typical satellite.

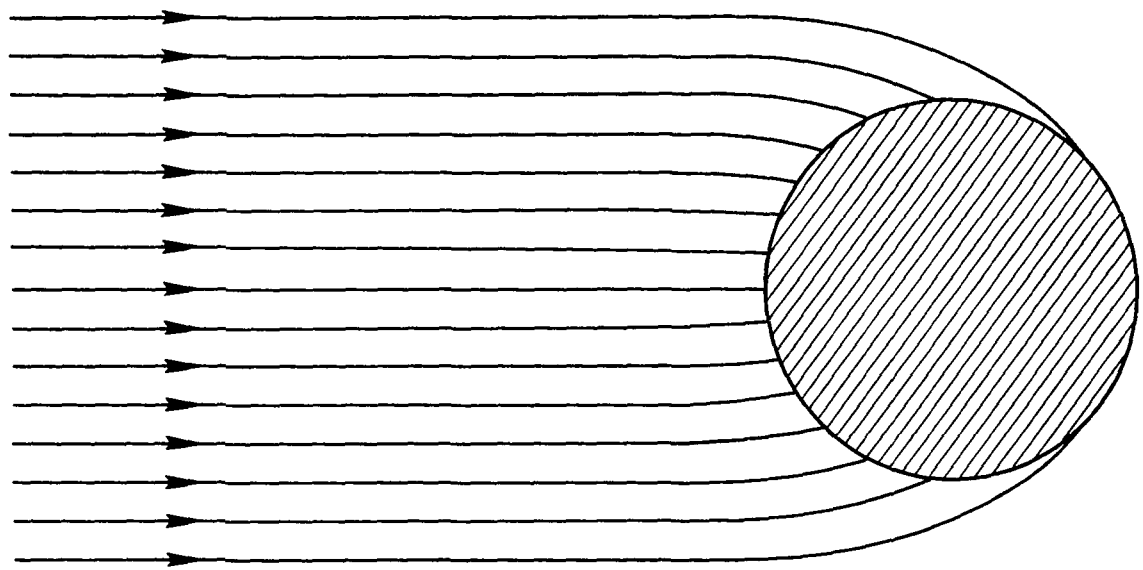

Figure 4.- Typical ion trajectories for model of this investigation; φ_o = -100 v, E = 100 ev, a = 1.25 cm.

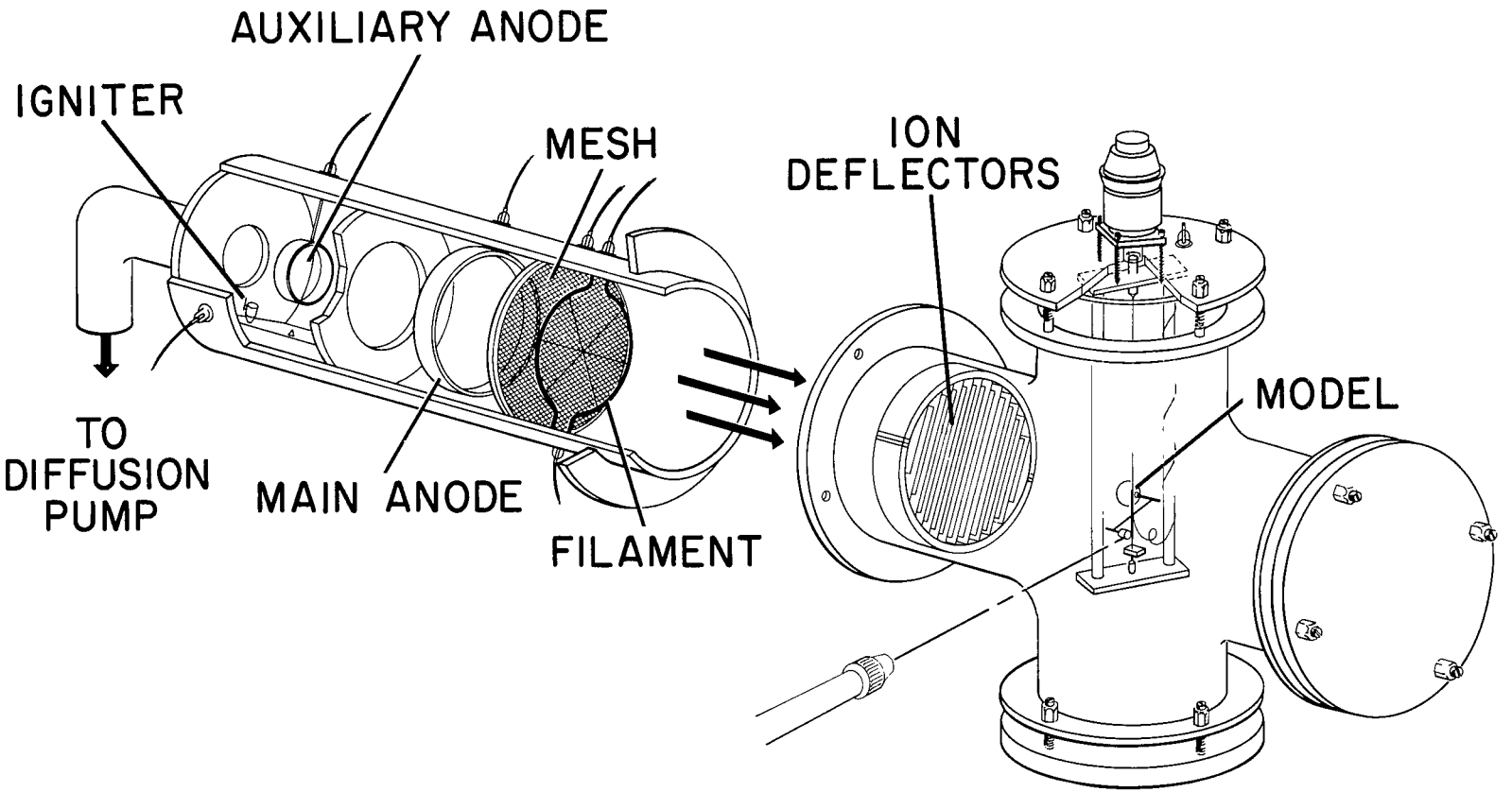

Figure 5.- Broad-beam plasma apparatus.

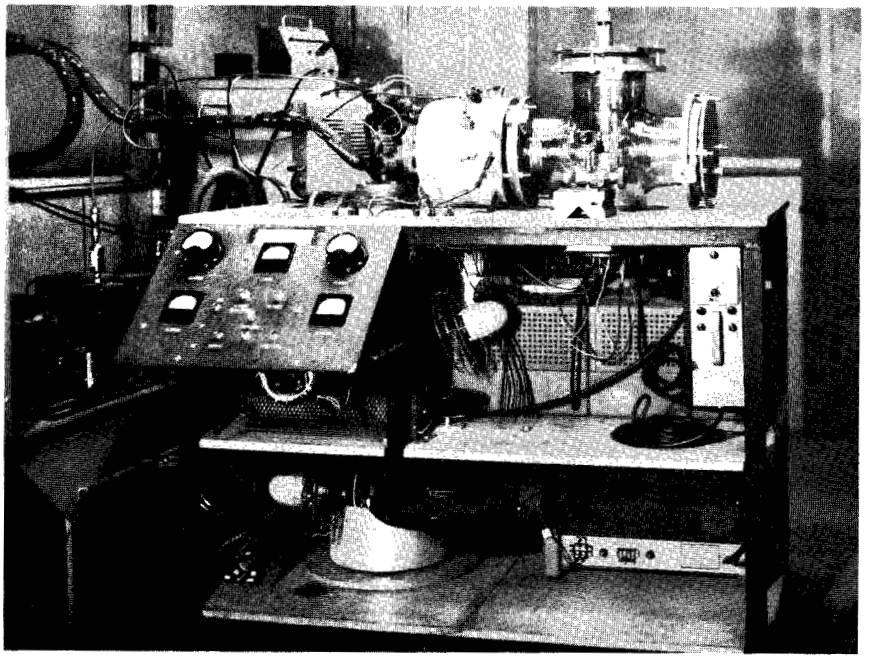

A-30066

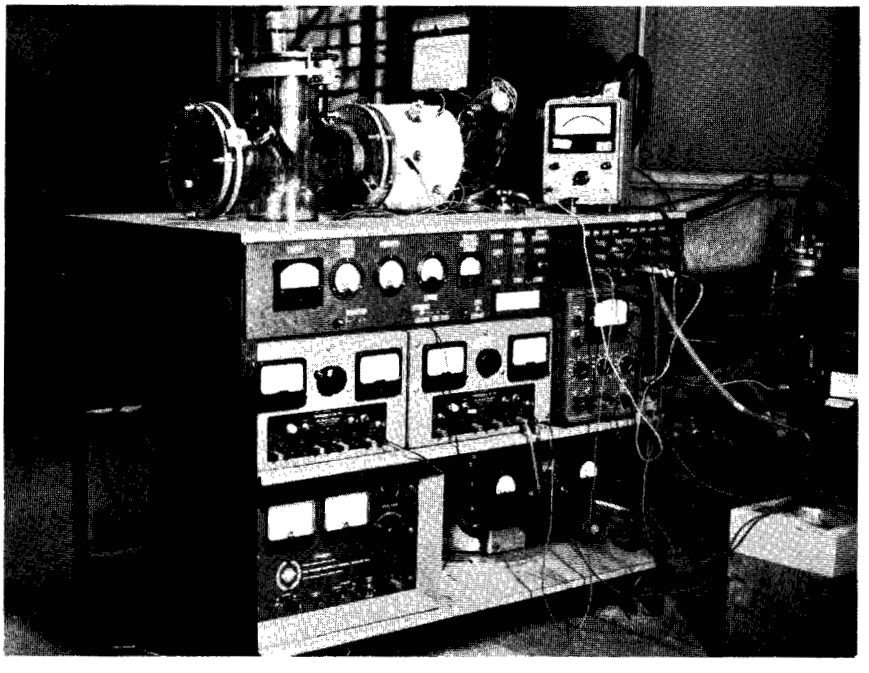

A-30067

Figure 6.- Two views of broad-beam plasma apparatus.

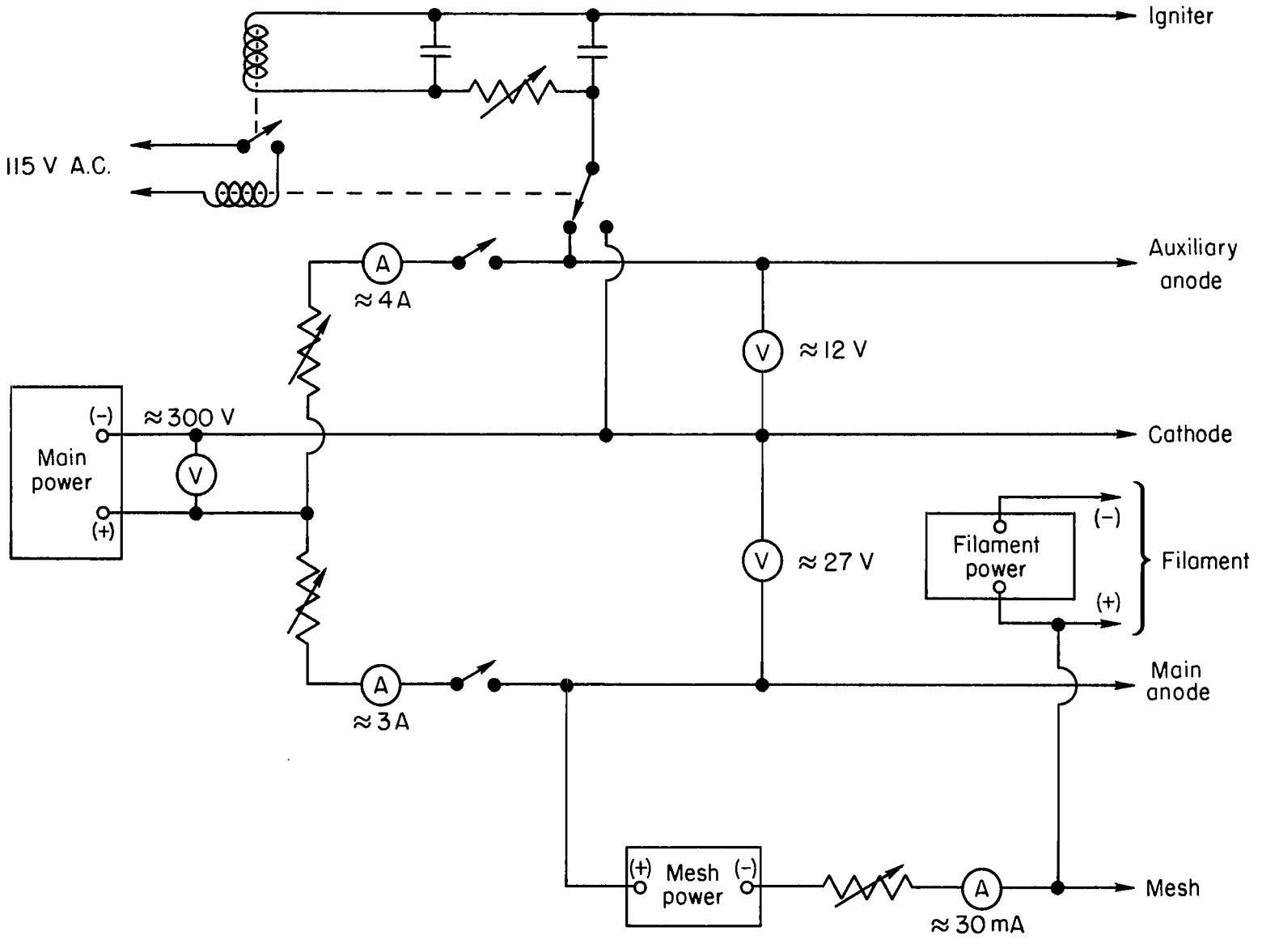

Figure 7.- Block circuit diagram of plasma discharge.

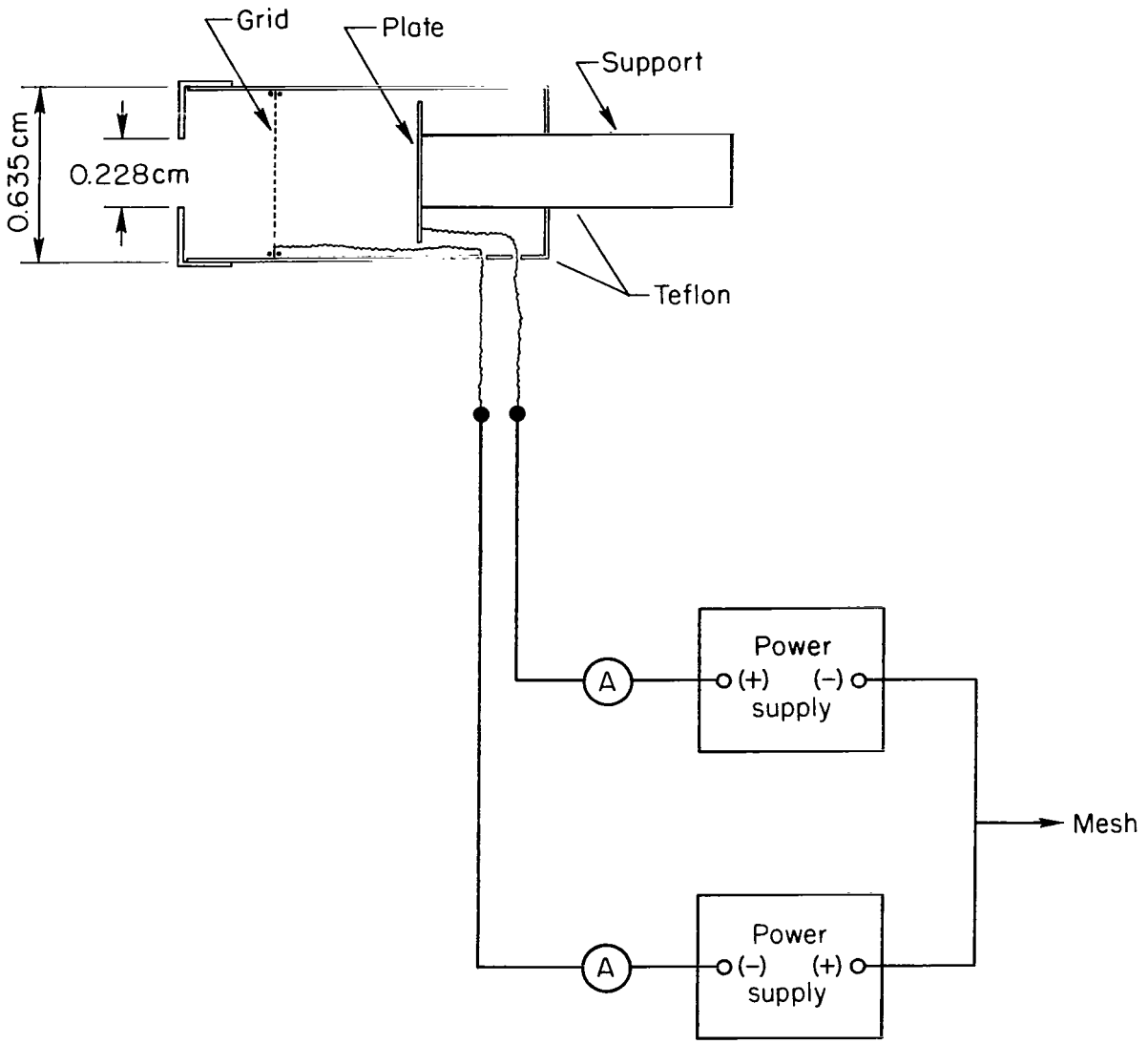

Figure 8.- Cross section and electrical circuit of Faraday cage.

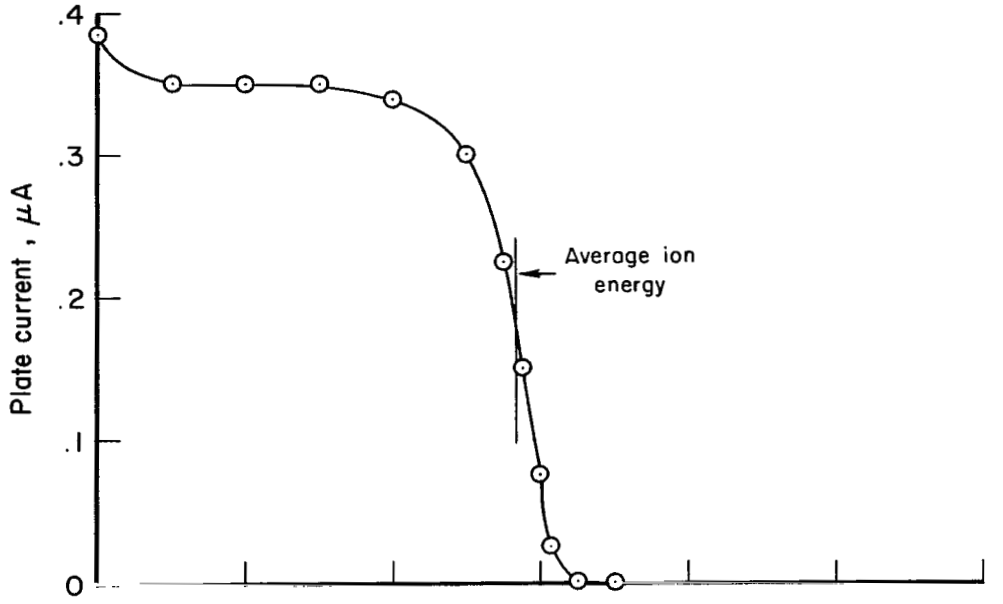

(a) Mesh potential = 120 volts.

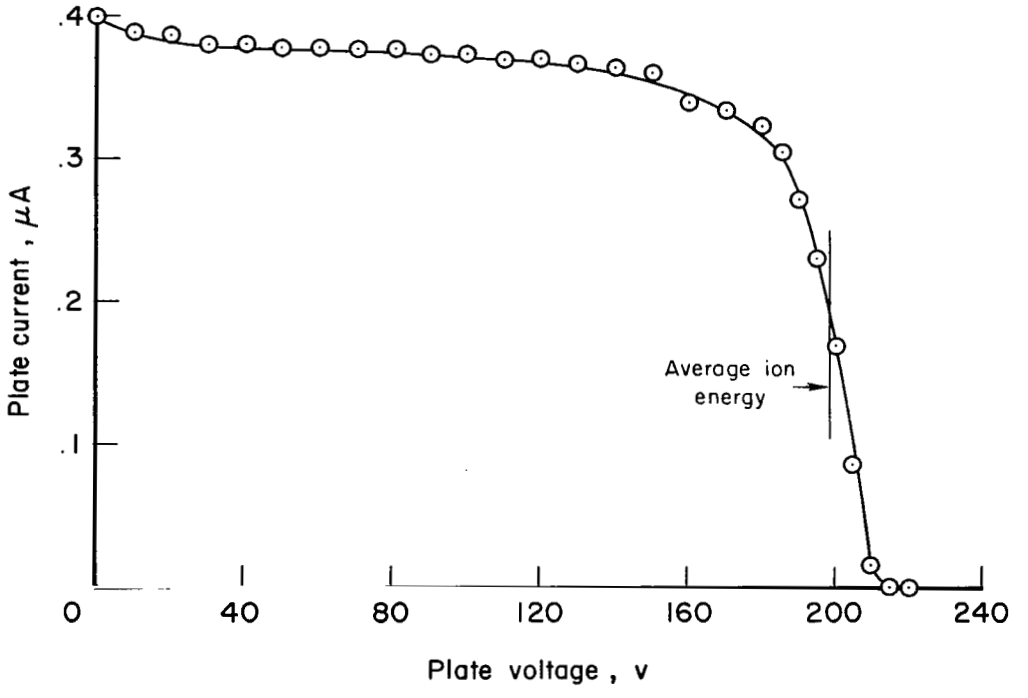

(b) Mesh potential = 210 volts.

Figure 9.- Ion energy spectrum from Faraday cage.

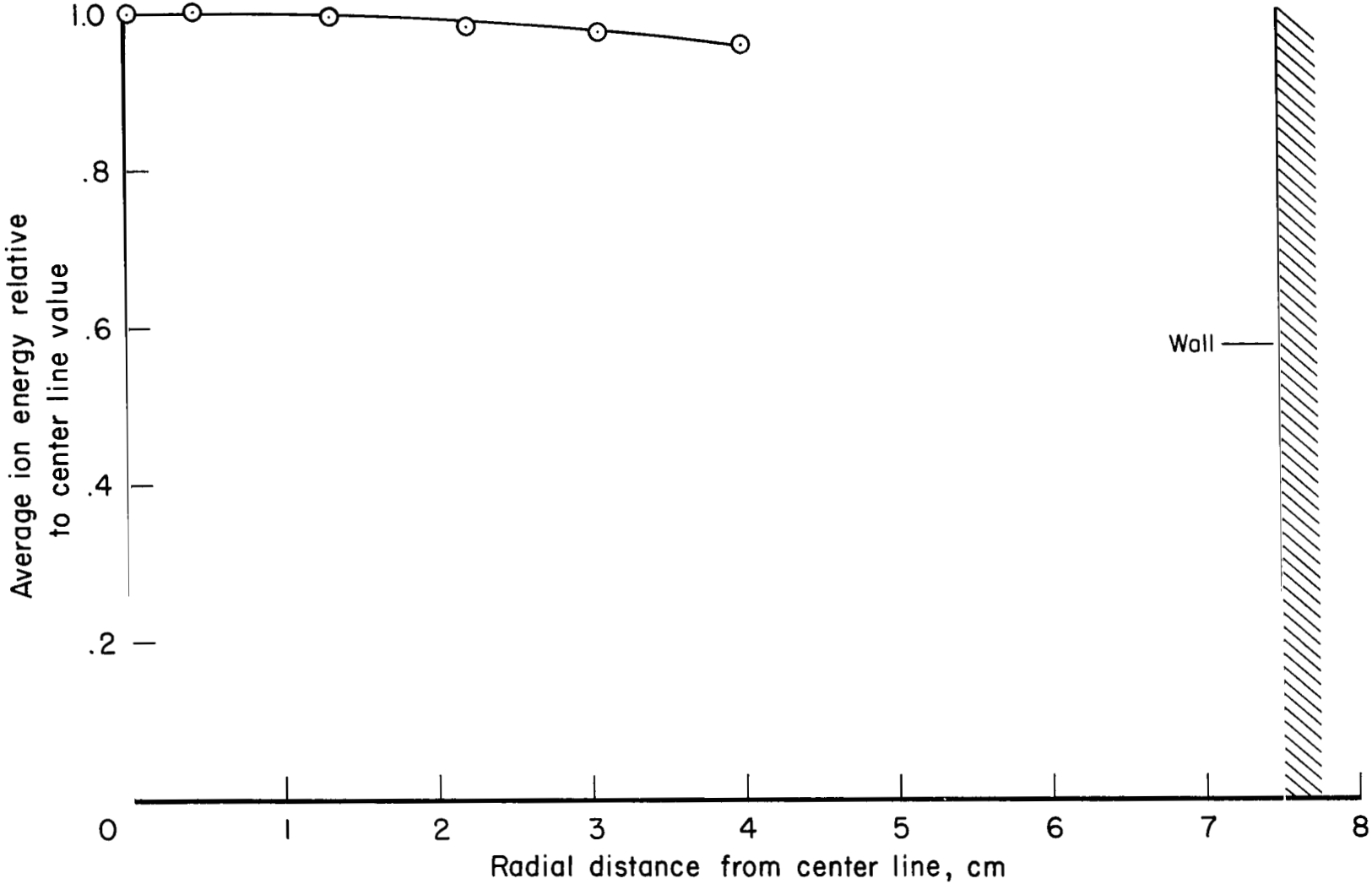

Figure 10.- Radial variation of average ion energy taken at axial position of the models.

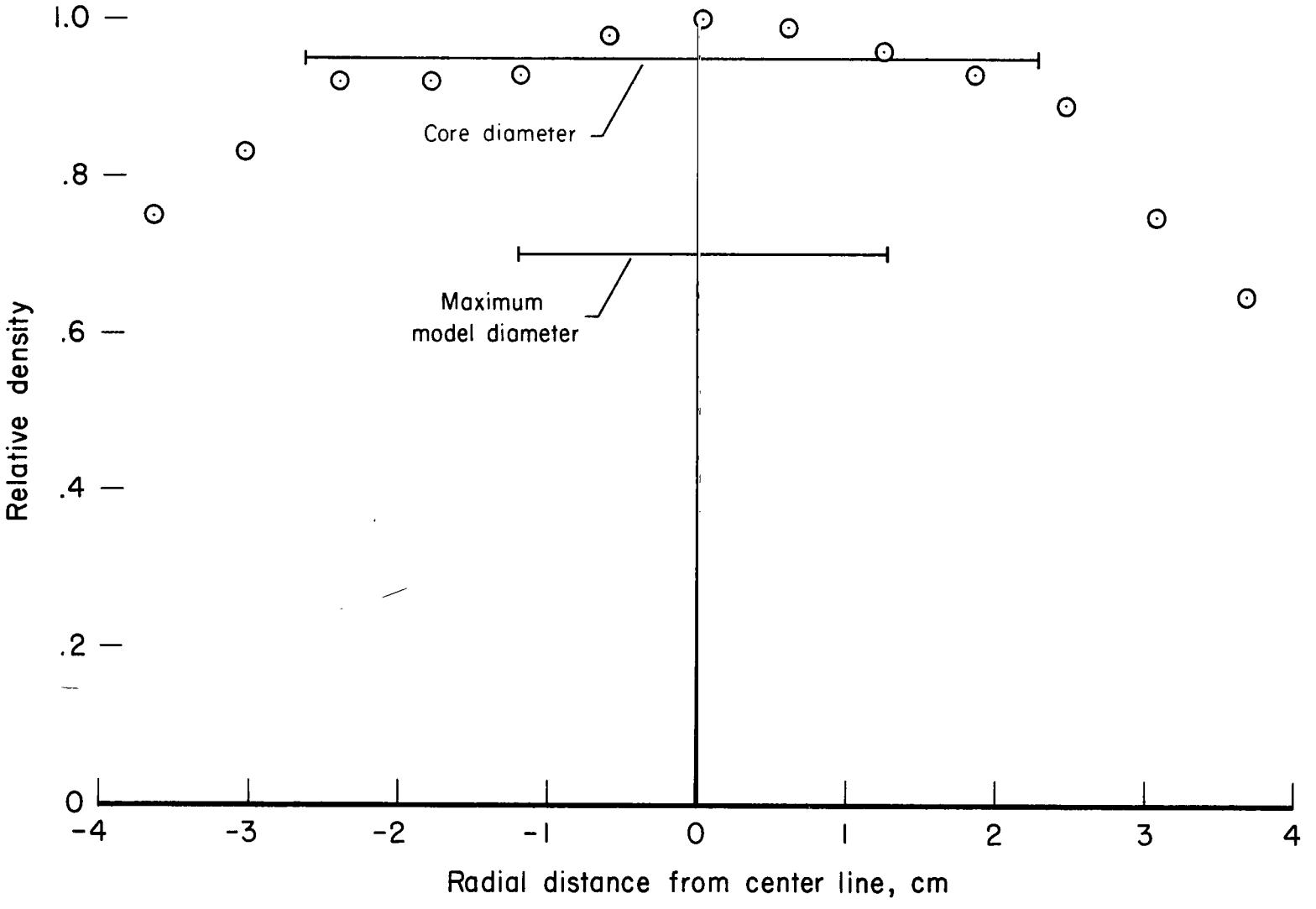

Figure 11.- Radial density distribution at axial position of models.

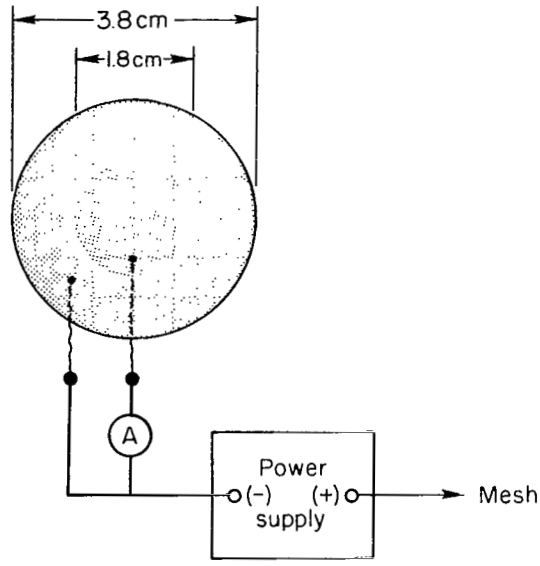

(a) Concentric-ring disk.

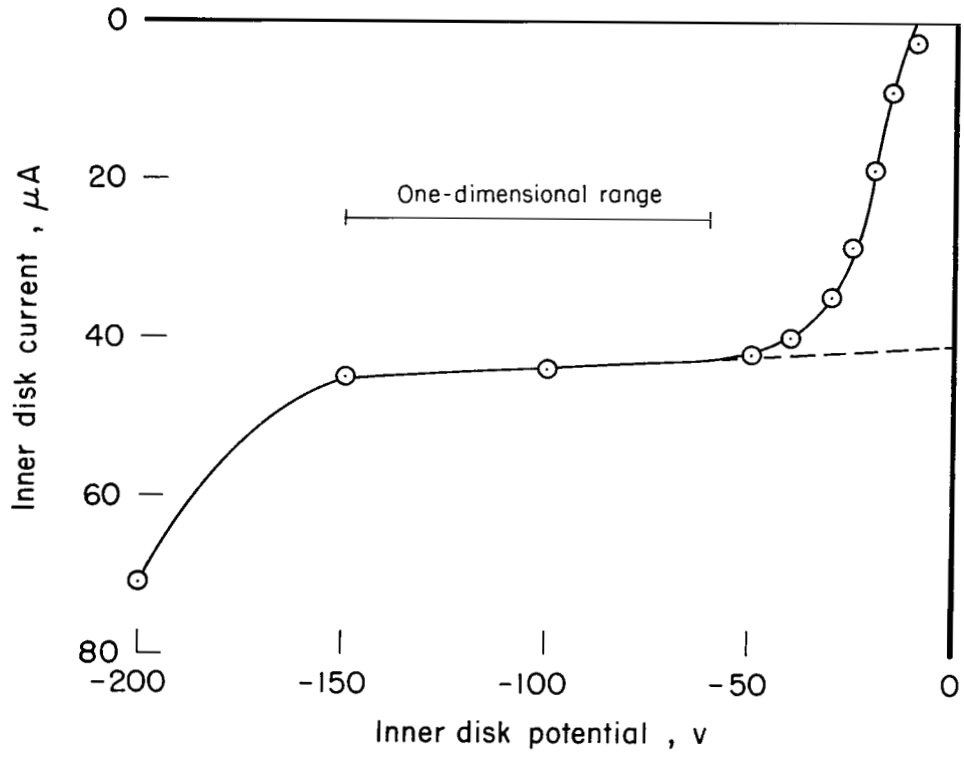

(b) Inner disk characteristic.

Figure 12.- Concentric-ring disk and characteristic.

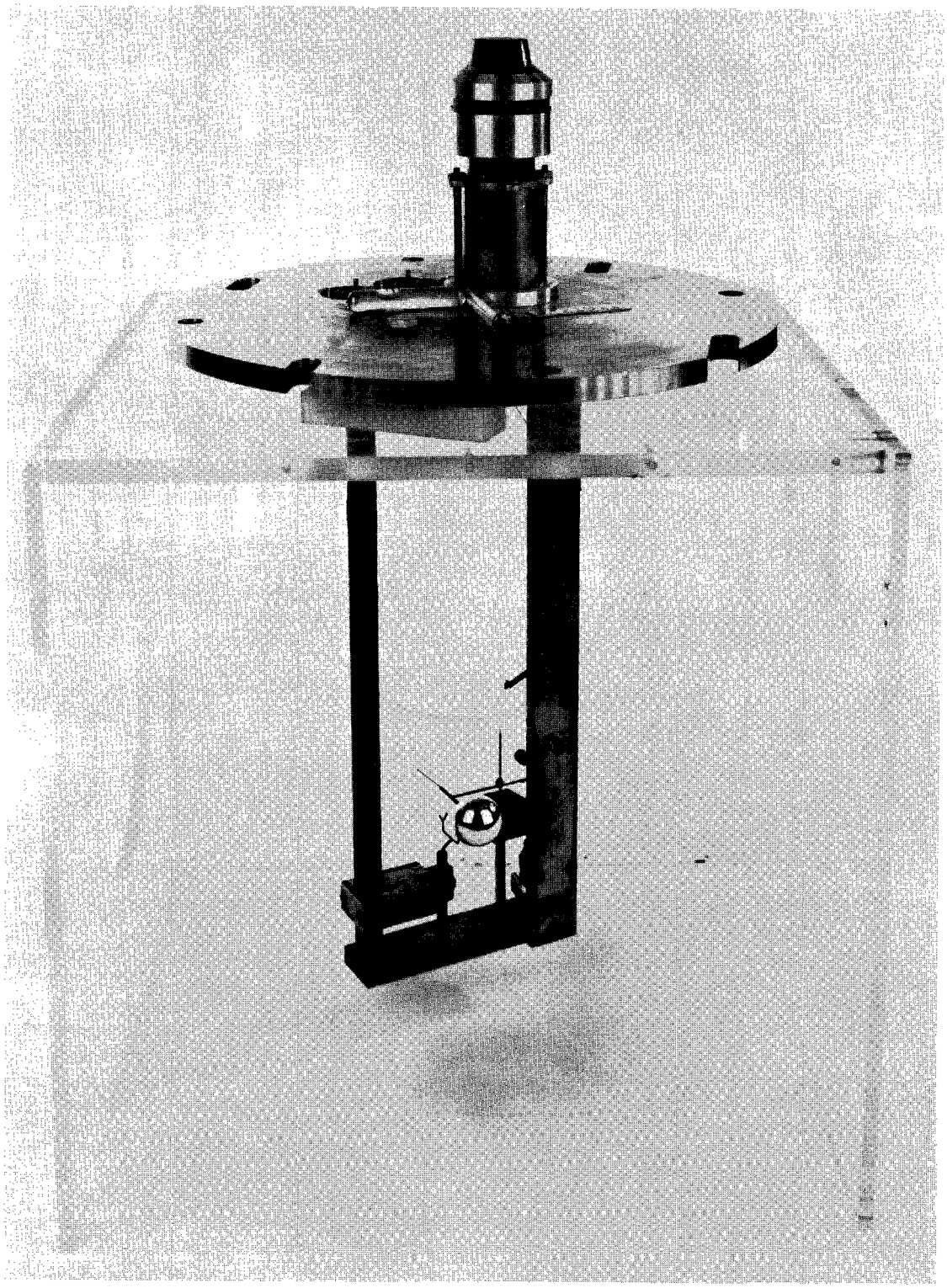

A-33184

Figure 13.- Quartz fiber microbalance.

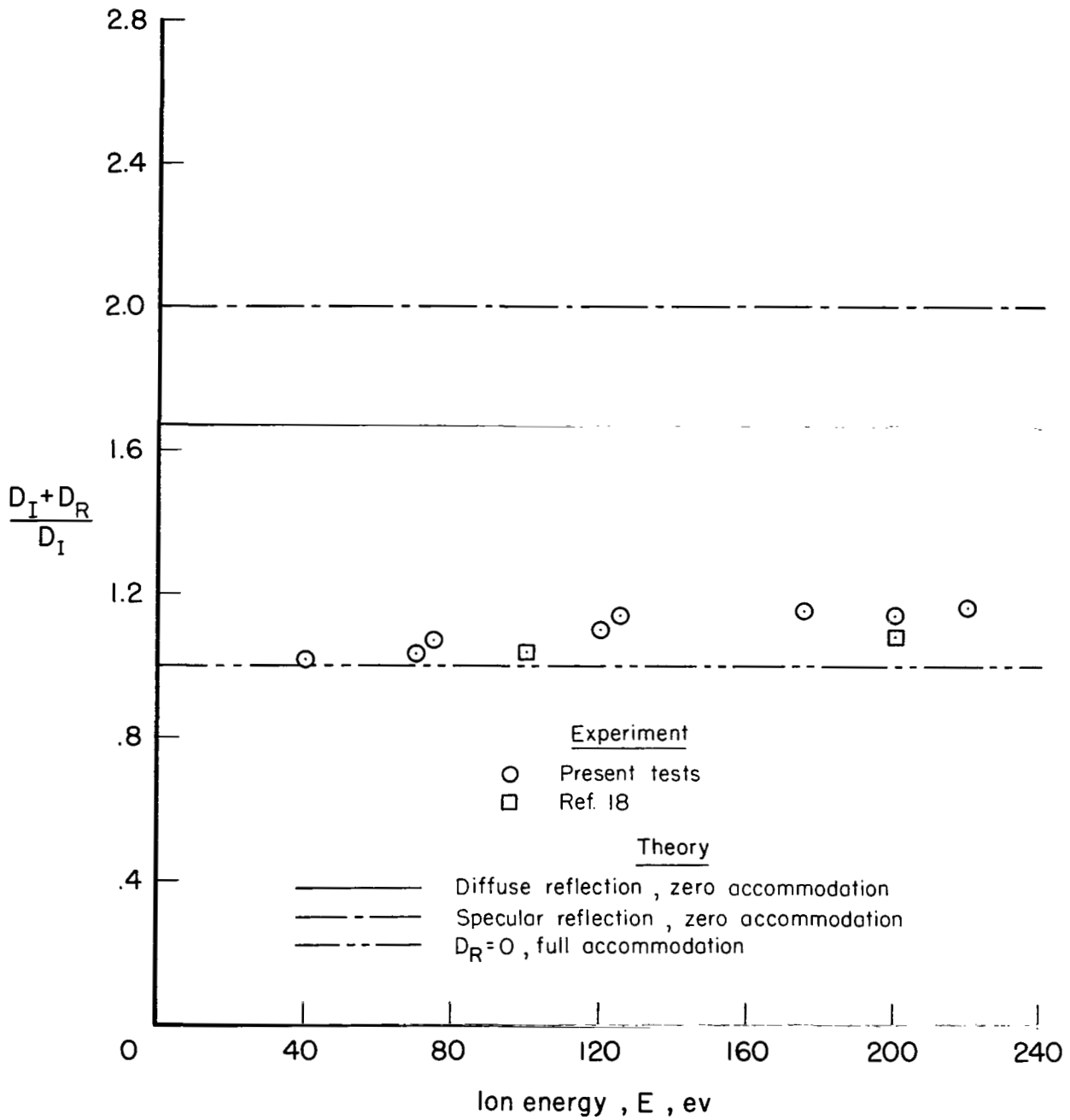

Figure 14.- Relative effect of reflection on drag of a flat plate at normal incidence, Hg^+ on Au.

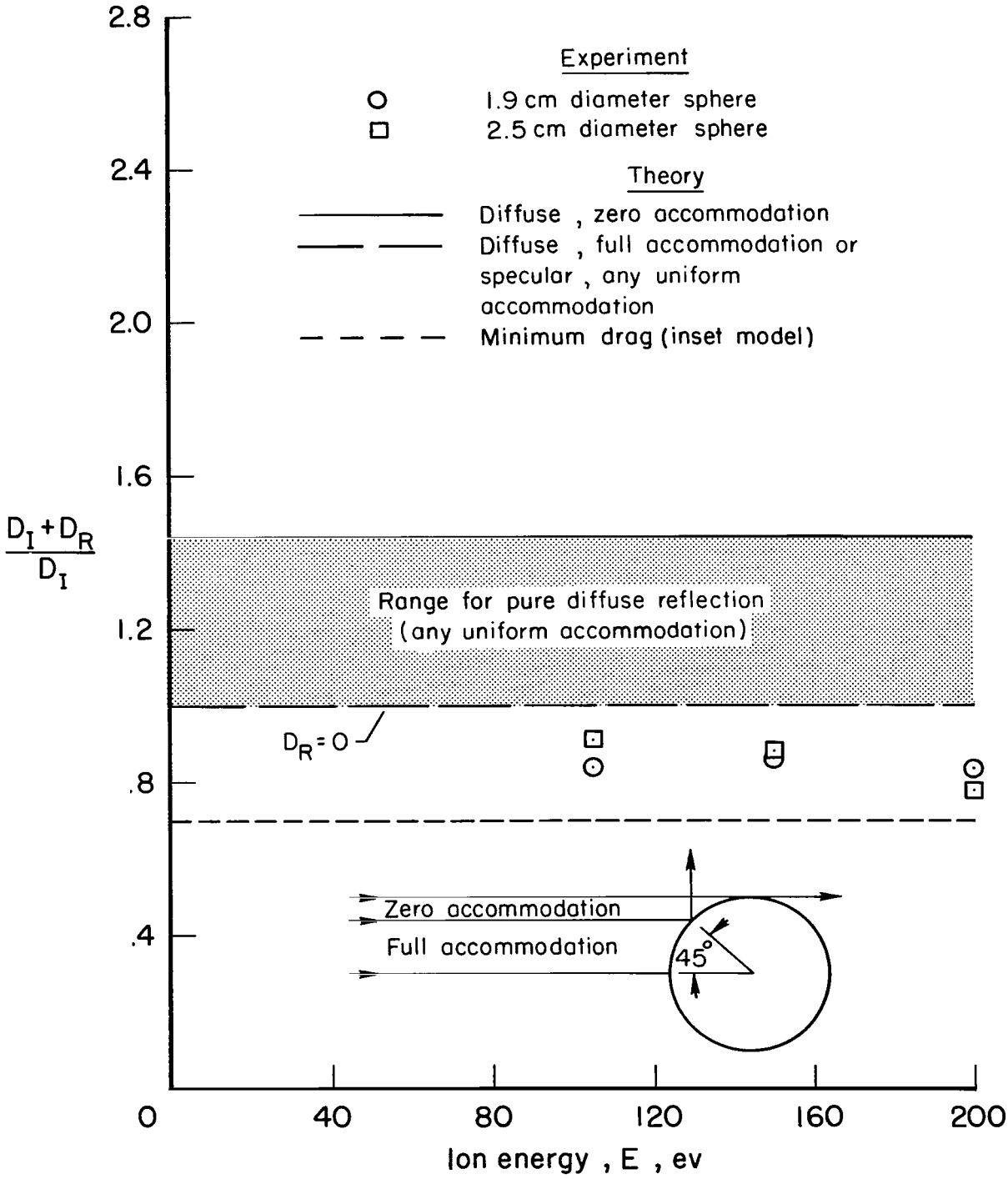

Figure 15.- Relative effect of reflection on drag of uncharged spheres, Hg^+ on Au.

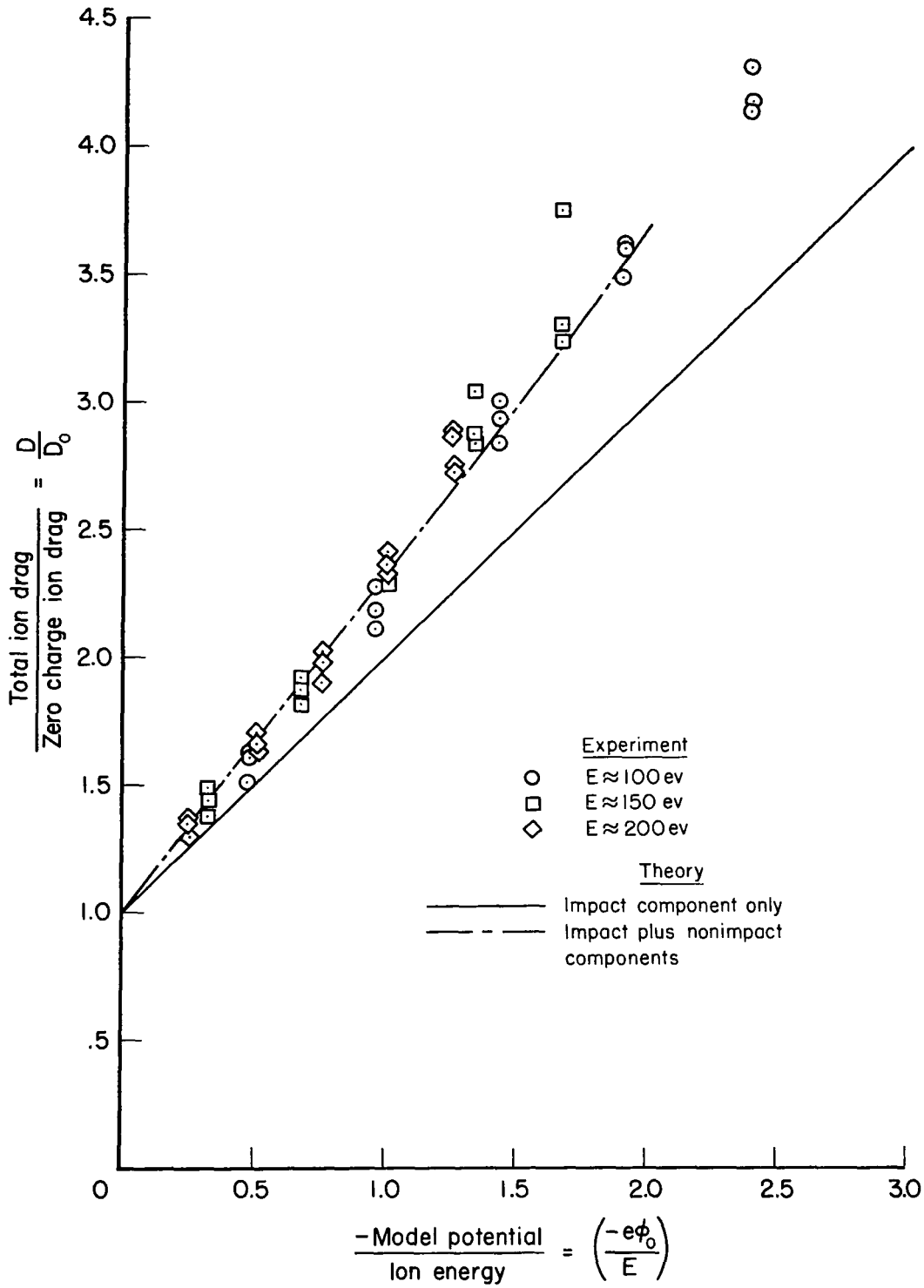

(a) Model diameter = 1.9 cm, $a/\lambda_D = 7.5$.

Figure 16.- Experimental electric drag and Jastrow-Pearse theory.

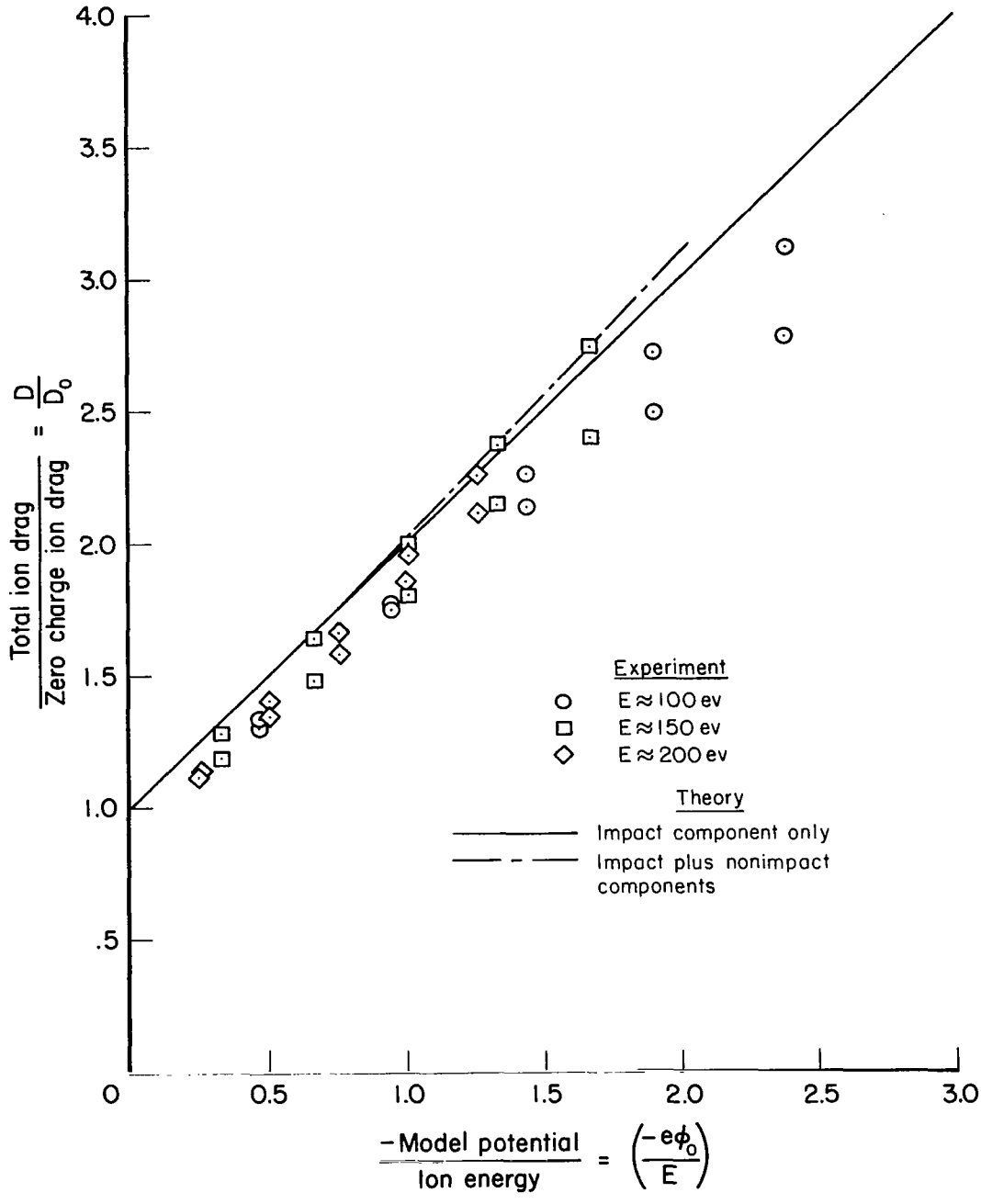

(b) Model diameter = 2.5 cm, a/λ_D = 10.

Figure 16.- Concluded.

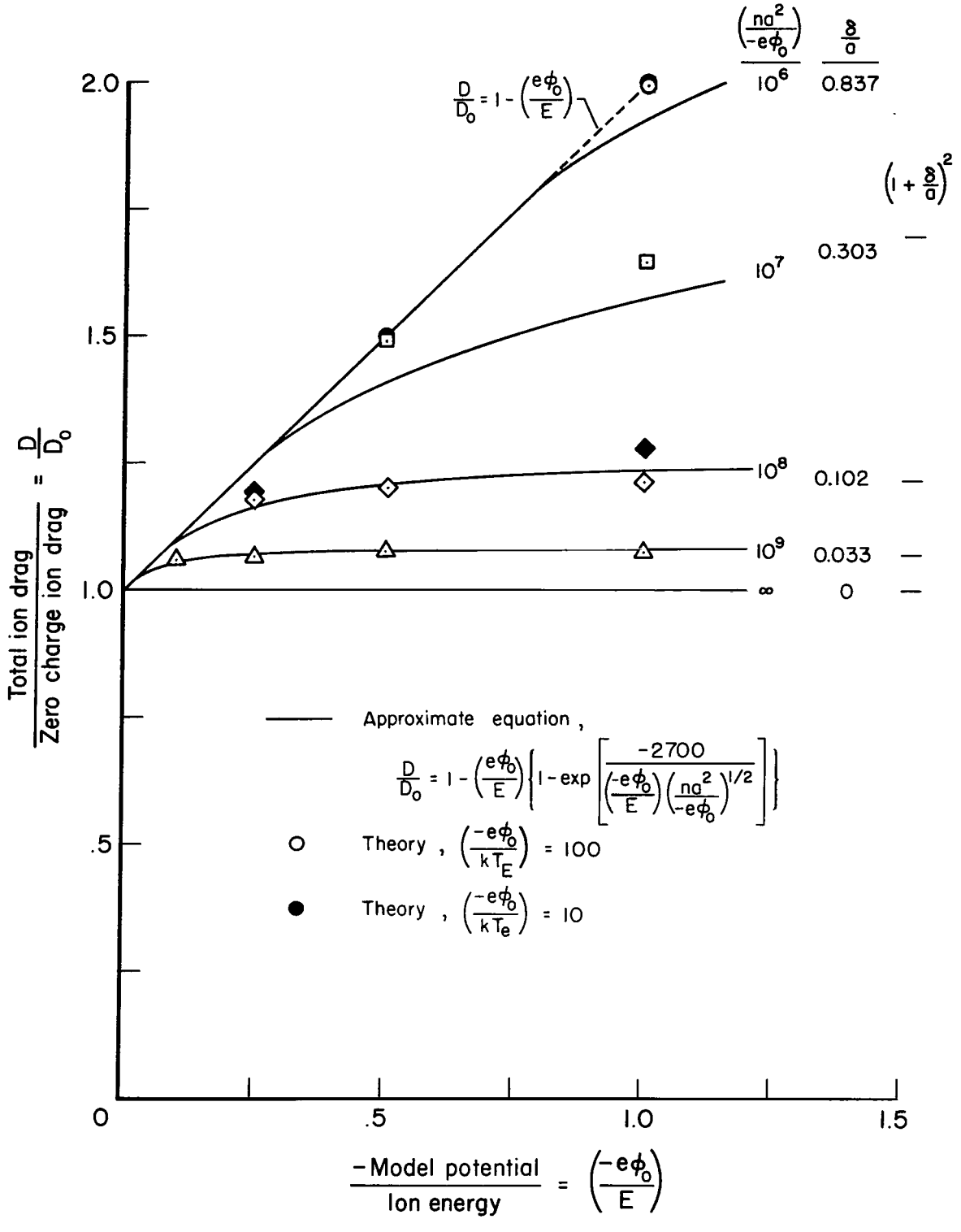

Figure 17.- Ion sphere drag as computed by Jastrow-Pearse theory and by approximate equation.

"The aeronautical and space activities of the United States shall be conducted so as to contribute . . . to the expansion of human knowledge of phenomena in the atmosphere and space. The Administration shall provide for the widest practicable and appropriate dissemination of information concerning its activities and the results thereof."

—NATIONAL AERONAUTICS AND SPACE ACT OF 1958

NASA SCIENTIFIC AND TECHNICAL PUBLICATIONS

TECHNICAL REPORTS: Scientific and technical information considered important, complete, and a lasting contribution to existing knowledge.

TECHNICAL NOTES: Information less broad in scope but nevertheless of importance as a contribution to existing knowledge.

TECHNICAL MEMORANDUMS: Information receiving limited distribution because of preliminary data, security classification, or other reasons.

CONTRACTOR REPORTS: Technical information generated in connection with a NASA contract or grant and released under NASA auspices.

TECHNICAL TRANSLATIONS: Information published in a foreign language considered to merit NASA distribution in English.

TECHNICAL REPRINTS: Information derived from NASA activities and initially published in the form of journal articles.

SPECIAL PUBLICATIONS: Information derived from or of value to NASA activities but not necessarily reporting the results of individual NASA-programmed scientific efforts. Publications include conference proceedings, monographs, data compilations, handbooks, sourcebooks, and special bibliographies.

Details on the availability of these publications may be obtained from:

SCIENTIFIC AND TECHNICAL INFORMATION DIVISION

NATIONAL AERONAUTICS AND SPACE ADMINISTRATION

Washington, D.C. 20546